Flood susceptibility mapping using multi-temporal SAR imagery and novel integration of nature-inspired algorithms into support vector regression

Mehravar, Soroosh; Razavi-Termeh, Seyed Vahid; Moghimi, Armin; Ranjgar, Babak; Foroughnia, Fatemeh; Amani, Meisam

DOI
10.1016/j.jhydrol.2023.129100

Publication date
2023

Document Version
Final published version

Published in
Journal of Hydrology

Citation (APA)
Mehravar, S., Razavi-Termeh, S. V., Moghimi, A., Ranjgar, B., Foroughnia, F., & Amani, M. (2023). Flood susceptibility mapping using multi-temporal SAR imagery and novel integration of nature-inspired algorithms into support vector regression. *Journal of Hydrology*, *617*(C), Article 129100. https://doi.org/10.1016/j.jhydrol.2023.129100

Journal of Hydrology 617 (2023) 129100

Contents lists available at ScienceDirect

Journal of Hydrology

journal homepage: www.elsevier.com/locate/jhydrol

Research papers

Flood susceptibility mapping using multi-temporal SAR imagery and novel integration of nature-inspired algorithms into support vector regression

Soroosh Mehravar [a], Seyed Vahid Razavi-Termeh [b], Armin Moghimi [c,d], Babak Ranjgar [c], Fatemeh Foroughnia [e,*], Meisam Amani [f]

[a] Department of Geomatics, University College of Engineering, University of Tehran, Tehran 1439957131, Iran
[b] Department of Computer Science & Engineering and Convergence Engineering for Intelligent Drone, XR Research Center, Sejong University, Seoul, Republic of Korea
[c] Faculty of Geodesy and Geomatics Engineering, K. N. Toosi University of Technology, Tehran 1996715433, Iran
[d] Institute of Photogrammetry and GeoInformation (IPI), Leibniz Universität Hannover (LUH), 30167 Hannover, Germany
[e] Department of Geoscience and Engineering, Civil Engineering and Geosciences Faculty, Delft University of Technology, Delft, the Netherlands
[f] Wood Environment & Infrastructure Solutions, Ottawa, ON K2E 7L5, Canada

ARTICLE INFO

Keywords:
Flood susceptibility mapping
Support vector regression (SVR)
Nature-inspired algorithms
SAR imagery
Remote sensing

ABSTRACT

Flood has long been known as one of the most catastrophic natural hazards worldwide. Mapping flood-prone areas is an important part of flood disaster management. In this study, a flood susceptibility mapping framework was developed based on a novel integration of nature-inspired algorithms into support vector regression (SVR). To this end, various remote sensing (RS) and geographic information system (GIS) datasets were applied to the hybridized SVR models to map flood susceptibility in Ahwaz township, Iran. The proposed framework has two main steps: 1) updating the flood inventory (historical flooded locations) using the proposed RS-based flood detection method developed within the google earth engine (GEE) platform. The mosaicked images of multi-temporal Sentinel-1 synthetic aperture radar (SAR) data have been used in this step; 2) producing flood susceptibility map using the standalone SVR and hybridized model of SVR. The hybridized methods were derived from a novel integration of SVR with *meta*-heuristic algorithms, hence forming the SVR-bat algorithm (SVR-BA), SVR-invasive weed optimization (SVR-IWO), and SVR-firefly algorithm (SVR-FA). A spatial database of flood locations and 11 conditioning factors (altitude, slope angle, aspect, topographic wetness index, stream power index, normalized difference vegetation index (NDVI), distance to stream, curvature, rainfall, soil type, and land use/cover) were built for the susceptibility modelling. The accuracy of the proposed model was evaluated using the statistical and sensitivity indices, such as root mean square error (RMSE), receiver operating characteristic (ROC) and area under the ROC curve (AUROC) index. The results indicated that all hybridized models outperformed the standalone SVR. According to AUROC values, the predictive power of the SVR-FA was the highest with the value of 0.81, followed by SVR-IWO, SVR-BA, and SVR with values of 0.80, 0.79, and 0.77, respectively.

1. Introduction

Flood is a natural disaster (Khosravi et al., 2016; Chen et al., 2020) with many socio-economic repercussions (Tien Bui et al., 2018), resulting in several other disasters, such as erosion, landslide, and sinkholes (Arabameri et al., 2019). Therefore, it is required to monitor floods using advanced techniques and develop accurate flood risk models (Samanta et al., 2018b).

To decrease the negative socio-economic effects of floods, it is important for governors and decision-makers to follow effective flood management plans. The most important part of flood management plans is to use the most accurate methods to identify and model the flood-prone areas within watersheds (Rahmati et al., 2016b; Tien Bui et al., 2018; Parsian et al., 2021). Contrary to flood prevention, which is not entirely possible, prediction of flood-prone areas is practical (Bui et al., 2016; Falah et al., 2019).

In general, methods used for flood susceptibility mapping can be categorized into four groups including physically-based models, multi-criteria decision analysis, statistical, and machine learning (Liu et al., 2021). The primary problem with physically-based models in several

* Corresponding author.
E-mail addresses: sorooshmehravar@ut.ac.ir (S. Mehravar), vrazavi70@gmail.com (S.V. Razavi-Termeh), moghimi@ipi.uni-hannover.de (A. Moghimi), babakranjgar@alumni.kntu.ac.ir (B. Ranjgar), f.foroughnia@tudelft.nl (F. Foroughnia), meisam.amani@woodplc.com (M. Amani).

https://doi.org/10.1016/j.jhydrol.2023.129100
Received 24 February 2022; Received in revised form 4 October 2022; Accepted 6 January 2023
Available online 20 January 2023

areas like Iran is that acquisition of various types of datasets is almost impractical due to many limitations (Shahabi et al., 2020). Physically-based models often need a significant level of computation and enough expertise to consider proper hydrological parameters (Mosavi et al., 2018). The multi-criteria decision analysis methods, such as the analytic hierarchy process are well-known for their simplicity making them widely used for flood susceptibility assessment. Multi-criteria decision analysis methods heavily rely on the judgement of experts, hence the results can inevitably be accompanied by subjectivities and uncertainties (de Brito et al., 2019).

Statistical methods generally include bivariate statistical analysis and multivariate statistical analysis (Liu et al., 2021). The frequency ratio (FR) is one of the most popular statistical bivariate statistical analysis methods (Ranjgar et al., 2021), which has frequently been used to estimate the influence of each class of factors on flooding. Logistic regression is also a common statistical multivariate statistical analysis method which can be used to determine the effect of conditioning factors on flooding. The predicted variables in these statistical methods are based on linear assumptions, while flood has generally been a phenomenon with a nonlinear structure (Liu et al., 2021).

The disadvantages of the physically-based models, multi-criteria decision analysis, and statistical models have led the researchers to use advanced data-driven models, such as machine learning algorithms, for studies of flood susceptibility modelling (Mosavi et al., 2018). The main reason that these models are more popular is because they can numerically formulate the complex nonlinearity of relationships between flood conditioning factors and flood potentiality. Among the machine learning methods, the artificial neural network (Tiwari and Chatterjee, 2010; Kim et al., 2016), neuro-fuzzy (Dineva et al., 2014), adaptive neuro-fuzzy inference system (ANFIS) (Pourghasemi et al., 2019), optimization of the ANFIS (Tien Bui et al., 2018), random forest (Wang et al., 2015), decision tree, support vector machine (SVM) (Suykens and Vandewalle, 1999; Tehrany et al., 2015a), and support vector regression (SVR) (Rahmati et al., 2020; Siam et al., 2021) have been widely employed for producing flood susceptibility maps. Many studies have attempted to incorporate the metaheuristic algorithms into the aforementioned machine learning methods to introduce near-optimal solutions at a reasonable computational cost. For instance, Termeh et al. (2018) investigated a combination of ANFIS with metaheuristic algorithms, including ant colony optimization, genetic algorithm, and particle swarm optimization (PSO) for flood susceptibility mapping. According to their results, the ensemble of ANFIS-PSO was the superior model in their study area. Pourghasemi et al. (2020) have also investigated the capabilities of combining ANFIS with four metaheuristic algorithms to flood zoning and assessments. Their results indicated that their proposed ensemble approaches were useful for flood hazard management.

Producing Flood susceptibility maps using SVM has increasingly been popular over recent years (Tehrany et al., 2015a, (Tehrany et al., 2019b,b)). The main reason is its generalization excellence (Choubin et al., 2019). The issue of the generalization problem implicates how well the trained system can predict the cases that were not the targets of training (Liu et al., 2021). Therefore, the generalization excellence helps to predict beyond the range of the training dataset. Moreover, SVM's independence from the subjective determination of weights (as opposed to multi-criteria decision analysis methods), and its capability to work without a large number of model parameters (as opposed to physically-based models) were the other reasons for its popularity. SVM has also been extended as a regression tool known as SVR (Ansari and Akhoondzadeh, 2020; Rahmati et al., 2020; Balogun et al., 2021). Generating Flood susceptibility maps using SVR models has frequently been reported to have successful results (Rahmati et al., 2020). However, the optimum determination of the SVR parameters is difficult and important. This challenge has led to the introduction of optimization-based SVR models. The remarkable outcomes of many novel-hybridized SVR methods (with regard to accuracy, generalization, uncertainty, performance, and robustness) have been reported in the literature (Hong, 2008; de Moel et al., 2015; Zhu et al., 2016; Young et al., 2017).

Historical flooded regions (flood inventory maps) are usually the foundation of flood susceptibility map generation (Samanta et al., 2018b; Tehrany et al., 2014). The flooded locations provided by field measurements are usually accurate. However, monitoring and modelling flood and flood-related parameters using in-situ data has many challenges, such as the limited number of measurements, coarse/inadequate spatial distribution, and outdated data. Due to such limitations, quick, large-scale and fine-resolution monitoring of the inundated areas using the traditional field measurements is almost impractical (Xu et al., 2020). Therefore, updated flood inventory maps are required to publicly identify the vulnerable areas that would be endangered in the near future flood events. The most practical way to quickly update a flood inventory is through remote sensing (RS) methods that use frequent near real-time data (Ngo et al., 2021).

Over recent years, large-scale hydrological data processing and accurate production of susceptibility maps have become feasible due to the recent developments in RS, geographic information system (GIS), machine learning, and cloud computing services (Tien Bui et al., 2018; Mahdavi et al., 2019; Shahabi et al., 2020). Large-scale flood studies inevitably have to cope with a vast quantity of data processing and computational complexity (Shafizadeh-Moghadam et al., 2018). Despite the significant advances in the RS field and the availability of time-series datasets, a major challenge is processing big geodata, which can be resolved by cloud computing platforms, such as the google earth engine (GEE) (Mehravar et al., 2021).

The specific geographical-climatic attributes of Iran, such as its large extent, abrupt climate changes, and spatially varying ranges of precipitation have intensively made it a flood-prone country. Flood damage in Iran has considerably increased over the past decades (Rahmati et al., 2016a; Termeh et al., 2018; Panahi et al., 2021). For example, the latest major floods in Iran, which occurred in February and March 2019, have caused 78 dead people and economic losses of about 1.8 billion USD. Particularly in the city of Ahwaz, these floods have caused thousands of partial/complete collapses of the structural systems and building shifts. Accordingly, 13 villages went thoroughly under water. Therefore, this study aims at flood susceptibility map production over the city of Ahwaz, Iran. As per the limitations of the current methods discussed above, the present study used the bitemporal ground range detected (GRD) product of Sentinel-1 SAR to update the outdated flood inventory maps. In this regard, a novel RS-based method for large-scale flood detection was developed in GEE. Then, a novel integration of SVR with three nature-inspired metaheuristic algorithms has been used to model flood susceptibility in Ahwaz. Aiming to fine-tune the parameters of the model, SVR was integrated with three metaheuristic optimization algorithms, including bat algorithm (BA), invasive weed optimization (IWO), and firefly algorithm (FA) algorithms.

2. Study area and data

2.1. Study area

Ahwaz is a city in the southwest of Iran (Fig. 1a) with a population of about 1,300,000. The city has an average elevation of 11 m above sea level. Ahwaz has an average temperature of 25 degreesC, and its average value of annual rainfall is 213 mm, indicating an arid climate region. The northern and central parts of Ahwaz contain flat and fertile plains, while its west and east halves have a considerable number of sandy hills. An infertile-dry plain is also extended from the south to the south-westernmost areas. Many high-risk riverine floods have occurred in this city over the recent years, and the latest dates back to April 2016, February 2019, April 2019, and November 2020, respectively (Fig. 1b).

One of the latest applications of RS as a flood warning system was the emergency declaration of the European commission's Emergency

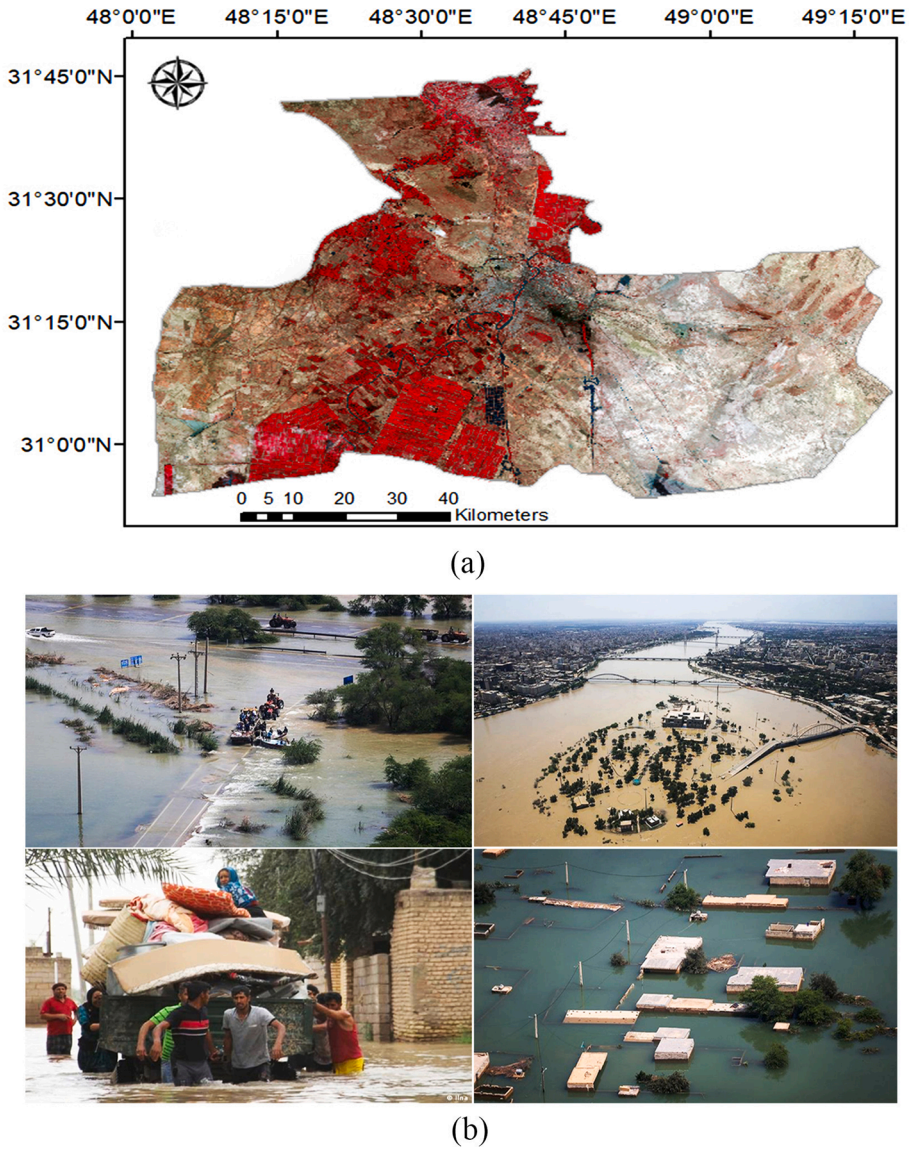

Fig. 1. Study area (Ahwaz city, Iran): (a) The location of the study area illustrated by the Landsat-8 true color composite image, and (b) The photographs of the past flood events in this city.

Response Coordinate Centre (ERCC) on the 1st of April 2019 for the case of Khuzestan province, Iran. According to the ERCC report, heavy rainfall was expected within 24 h after the 1st of April 2019, leading to large amounts of water moving downstream into the province of Khuzestan and potentially causing rivers to overflow their banks.

2.2. Datasets

In this study, the VV polarization of the Sentinel-1 GRD data with a spatial resolution of 10 m was used for flood mapping. The GRD products used in this study were two mosaicked images, among which the first one corresponded to the time before the flood event (mosaic of the images acquired on March 11th,2019 and March 24th, 2019). The second one corresponded to the time of the sequential flood event (mosaic of the images acquired on April 7th, 2019 and April 16th, 2019). In this study, the flood map of the Copernicus emergency management service (website address: https://www.erccportal.jrc.ec.europa.eu) for the city of Ahwaz (for the same flood event) was used to evaluate the accuracy of the produced flood maps.

3. Method

The workflow of the proposed method (Fig. 2) is divided into two main sections: (1) The flood detection methodology for producing and updating flood inventory maps; and (2) The modelling approach which was used for flood susceptibility map production. In general, the main steps of the proposed method are: (1) An updated flood inventory map is generated using a novel flood detection method applied to Sentinel-1 SAR data within the GEE platform (section 3.1); (2) A spatial database was formed using the produced flood inventory and the layers of the flood conditioning factors; (3) The multi-collinearity test and ReliefF algorithms were used to analyze the suitability and relative importance of the flood conditioning factors. The frequency ratio (FR) model was then used to assess the effect of each flood conditioning factor on flood occurrences; (4) The flood inventory derived from GEE was categorized into training (70 %) and testing (30 %) samples; (5) The training samples were utilized to optimize the parameters in the SVR using the BA, IWO, and FA *meta*-heuristic algorithms; (6) The susceptibility maps were separately produced using the SVR, BA-SVR, IWO-SVR, and FA-SVR algorithms; (7) The generated flood susceptibility maps were evaluated using root mean square error (RMSE) and the receiver operating

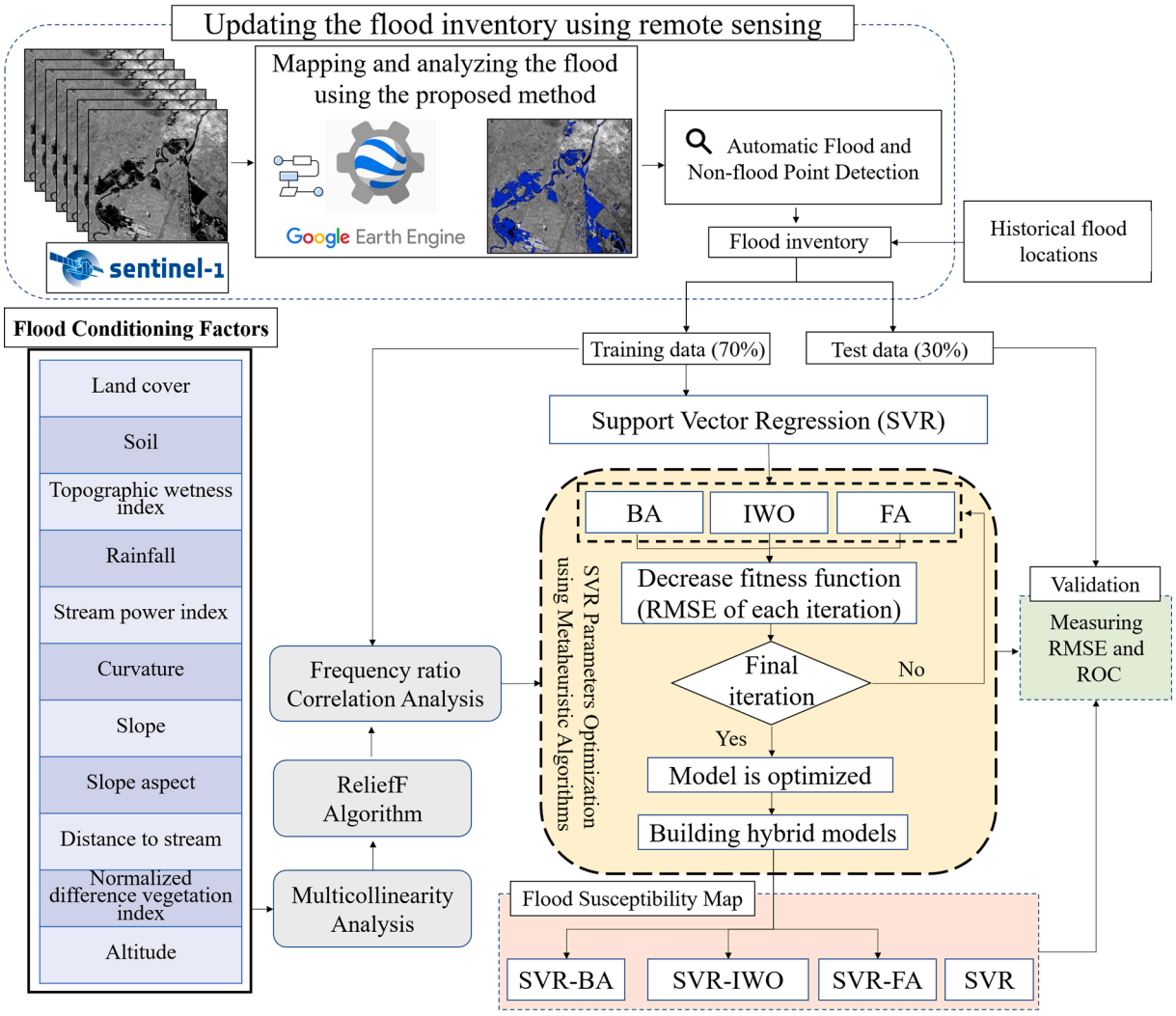

Fig. 2. The block diagram of the proposed methodology.

characteristic (ROC) curves.

3.1. *Updating the flood inventory using the proposed flood mapping algorithm*

The initial flood inventory map was obtained from two sources. The first source was the historical flood locations provided by the local agricultural department. These datasets include the locations that have frequently been affected by floods. The second source was a flood map generated using the proposed method. Since the proposed flood mapping method benefits from the ready-to-use Sentinel-1 datasets and processing power of GEE (https://earthengine.google.com/platform), it can be a practical choice for mapping large floods which require heavy computation of massive data. As depicted in Fig. 3, the proposed method for flood detection had five main steps: (1) SAR data preprocessing; (2) change detection; (3) water body detection; (4) flood inventory generation; and (5) validation. These steps are briefly explained below.

In the first step, two subsets of the same descending/ascending Sentinel-1 data were extracted from GEE data collection (pre-flood SAR image (I_1) and post-flood SAR image (I_2)). Afterwards, the VV polarization of these images was employed for further processing of flood detection. Many studies in the literature have reported that slightly higher thematic accuracies could be obtained using the VV polarization instead of the VH polarization for flood mapping/monitoring (Twele et al., 2016; Martinis et al., 2018). This is mainly due to the better contrast between water and no-water areas in the VV polarization data. To reduce the intrinsic speckle-effect of pre-and post-flood images, $I_{1,VV}$ and $I_{2,VV}$, a smoothing filter with a window size of 7*7 was utilized.

In the second step, a reliable binary change map of floods was produced by applying an appropriate decision function on a difference image. To this end, the bitemporal smoothed images of $I_{1,VV}$ and, $I_{2,VV}$, were first utilized to generate three difference images generated by the normalized difference flood index (Cian et al., 2018), log ratio index, and mean ratio index (Moghimi et al., 2017a) as follow:

$$\text{mean ratio index} = 1 - min\left(\frac{mean(\sigma_{0I1,VV})}{mean(\sigma_{0I2,VV})}, \frac{mean(\sigma_{0I2,VV})}{mean(\sigma_{0I1,VV})}\right) \quad (1)$$

$$\log ratio\ index = \left|\ln\left(\sigma_{0I2,VV}/\sigma_{0I1,VV}\right)\right| = \left|\ln\left(\sigma_{0I2,VV}\right) - \ln\left(\sigma_{0I1,VV}\right)\right| \quad (2)$$

$$\text{normalized difference flood index} = \frac{mean(\sigma_{0I1,VV}) - min\left(\sigma_{0I1,VV} + \sigma_{0I2,VV}\right)}{mean(\sigma_{0I1,VV}) + min\left(\sigma_{0I1,VV} + \sigma_{0I2,VV}\right)} \quad (3)$$

Where *mean*(.) and *min*(.) refers to the 'local mean' and 'minimum' operators. Although the mean ratio index can well highlight the changed/flooded regions, it intensifies noise and artifacts. On the other hand, the log ratio index is usually robust to residual speckle-effect owing to log transformation in converting the multiplicative noise to additive noise (Moghimi et al., 2017b). However, the changed/flooded regions and their boundaries are less highlighted in this index. In

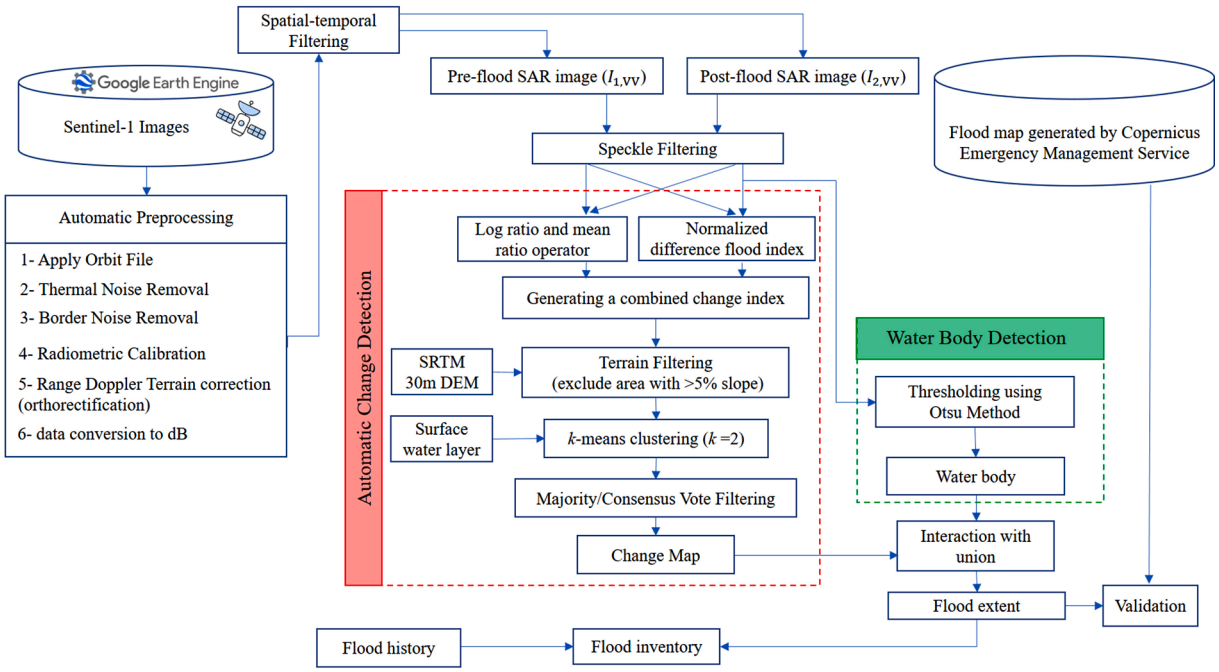

Fig. 3. The flowchart of the proposed flood mapping method.

addition to the advantages and disadvantages of the log ratio index and mean ratio index, they do not completely embody the nature of the scattering behavior of SAR images in detecting flooded regions. In this regard, the normalized difference flood index reflects more accurate structural information for flooded regions, resulting in better differentiation of these areas than non-smooth surfaces (e.g., urban zones, forests, and agriculture) (Cian et al., 2018). This can be mainly due to the simultaneous use of ratio and minimum operators in the normalized difference flood index equation. Nevertheless, noise-like patterns (anomalies) are highlighted more in this index compared to the log ratio index, resulting in a noisy change map. Moreover, some geometrical details of changed/flooded areas may be lost in the normalized difference flood index, resulting in miss detection errors.

In general, a single index cannot accurately demonstrate the information of the flooded regions and their geometric details. Aiming to address this issue, we strengthen the normalized difference flood index by combining it with the log ratio index and the mean ratio index based on a simple operator (the second root of multiplying) to generate a single ideal difference index as the proposed method (Eq. (4)). Using the proposed method, flooded regions can be detected with better accuracy and anomalies can be lessened.

$$\text{proposed method} = \sqrt{\left(\frac{\text{mean ratio index} + \text{log ratio index}}{2}\right).\text{normalized difference flood index}} \quad (4)$$

In this study, the proposed method was adjusted further using the SRTM DEM from pixels with slope values>5 %. Subsequently, a change map was produced by applying the k-means algorithm (MacQueen, 1967) with k = 2 (referring to change and no-change classes) to the refined difference index. Finally, the surface water layer was excluded from the change map to generate an ideal map, specialized for flood detection applications.

Besides the flooded areas, the change map might include the other land cover changes, resulting in false detection. The water body map derived from a post-flood image should be masked from the change map to reduce such false alarms. In this study, the water body was first detected by applying Otsu thresholding (Otsu, 1979) on the post-flood SAR image, $I_{2,VV}$. The flood extent map was then produced by intersecting the change map and water body map. Then, it was evaluated by the flood map provided by the Copernicus emergency management service. Finally, the flood inventory map was produced by adding new locations from the flood extent map to the historical flood points.

3.2. Flood conditioning factors

The selection of the optimal flood conditioning factors is a prerequisite for producing flood susceptibility maps. In this study, based on the results of previous studies (Arabameri et al., 2019; Janizadeh et al., 2019; Kalantar et al., 2021), 11 flood conditioning factors (Fig. 4) including altitude, slope angle, aspect, topographic wetness index, stream power index, normalized difference vegetation index (NDVI), distance to stream, curvature, rainfall, soil type, and land cover were employed. Among the selected factors, altitude is of considerable importance, which has been reported to be a key factor in many previous studies (Tehrany et al., 2014; Dodangeh et al., 2020). Some of the aforementioned flood conditioning factors, including altitude, curvature, distance to streams, slope angle, aspect, stream power index, and topographic wetness index were produced from the 30 m SRTM DEM. The altitude range in the study area is very low (-3 to178 m), and the region is mostly covered by flat plains, farmlands, and bare lands. The slope is an important factor that controls the velocity of water on the ground surface, hence affecting the infiltration and runoff. In fact, the infiltration depth is high and the runoff is low wherever the slope is low (Al-Juaidi et al., 2018). Curvature has also been reported to have the

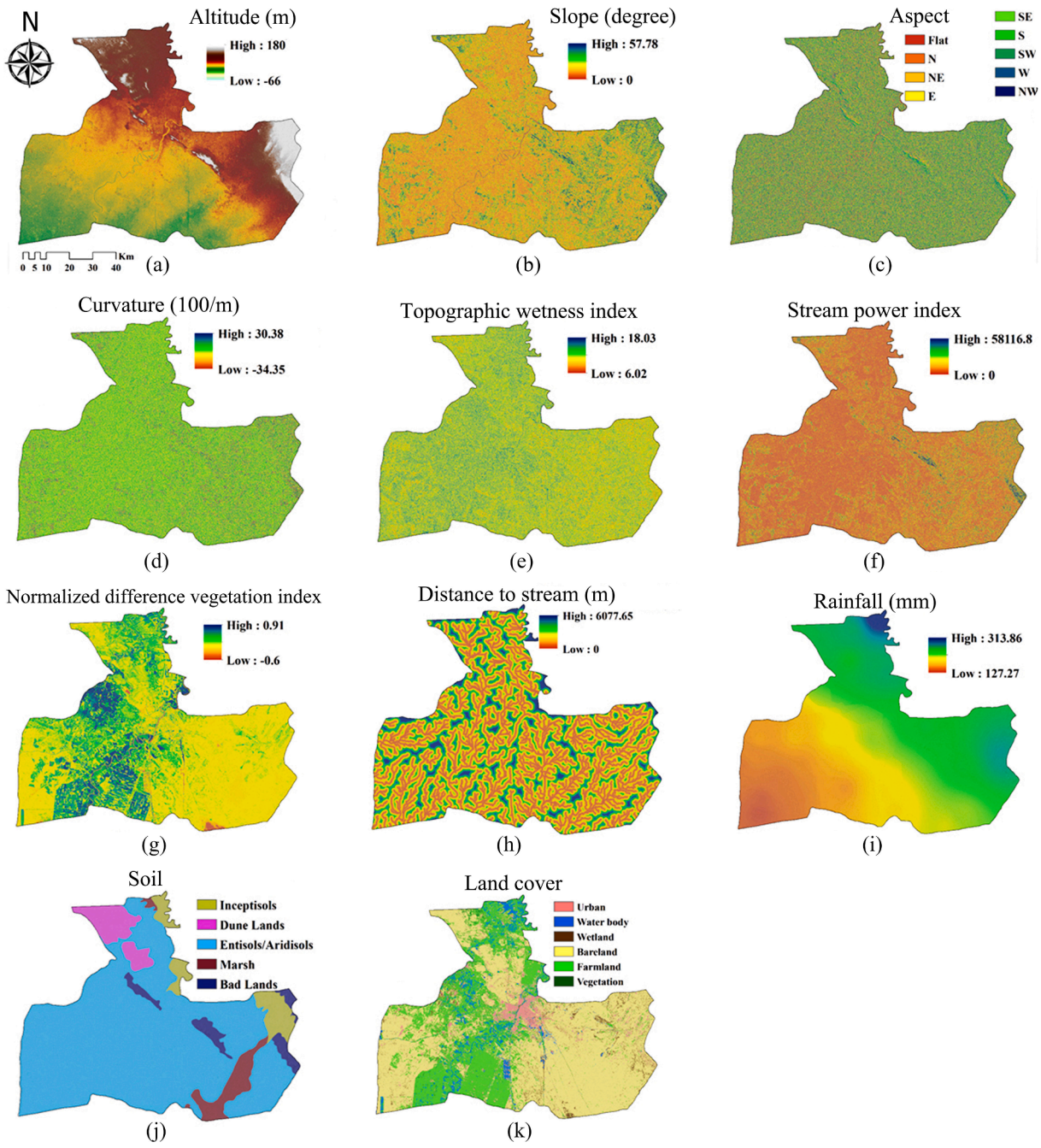

Fig. 4. The maps of the flood conditioning factors, including (a) altitude, (b) slope, (c) aspect, (d) curvature, (e) topographic wetness index, (f) stream power index, (g) NDVI, (h) distance to stream, (i) rainfall, (j) soil, and (k) land cover.

potential to influence flood occurrences, surface runoff and infiltration (Cao et al., 2016; Chapi et al., 2017).

The distance to stream factor is reported to have a substantial effect on flood extent and severity (Termeh et al., 2018). The hydrological flood conditioning factors, such as the stream power index and topographic wetness index also play a key role in the flood models. Since the stream power index can denote the potential of the stream to trigger erosion, it plays an imperative role in terrain stability level, hence being a widely used factor in most flood modelling studies. The topographic wetness index can also be used to quantify the topographical impact on hydrological processes (Tehrany et al., 2019a), and it is computed by dividing the specific basin area by the region slope (Arora et al., 2021). The topographic wetness index and stream power index have been calculated from DEM in QGIS using Eq. (5) and (6).

$$\text{topographic wetness index} = \ln\left(\frac{A_s}{\beta}\right) \tag{5}$$

$$\text{stream power index} = A_s * \tan\beta \tag{6}$$

where A_s shows the particular catchment area and β denotes the slope angle. The stream power index indicates the erosive power of surface runoff. In this study, the land cover map of the study area with a spatial resolution of 10 m was used (Ghorbanian et al., 2020). Moreover, the rainfall thematic layer was derived from the last decade of rainfall data in the region (stations of the region). Heavy rainfall is reported to be the main factor for floods occurrence (Samanta et al., 2018a)(Khosravi et al., 2019a,b). The rainfall thematic layer was acquired from the Khuzestan meteorological organization based upon the data over the

2010–2020 period, provided from stations in the city of Ahwaz. The inverse distance weighted technique was applied in this study to interpolate rainfall values. The soil type conditioning factor was also selected due to its noticeable effect on runoff risk. Since the infiltration of water mainly relies on soil texture, the soil type can be an effective parameter for the activation of hydrological processes. The soil type formation layer was obtained from the pedological map of Ahwaz at 1:100,000 scale. The soil data were classified into five classes, including Inceptisols, Dune lands, Entisols/Aridisols, Marsh, and Badlands. According to the literature, there is a negative relation between flooding and vegetation density. Therefore, the NDVI can be considered an appropriate factor to show the relationship between flooding and vegetation in a basin. The NDVI map of the study area was produced from the Landsat 8 OLI imagery for the year 2019 using Eq. (7), and its values varied between −0.6 and 0.91.

$$\mathrm{NDVI} = \frac{nearinfrared - red}{nearinfrared + red} \tag{7}$$

3.3. Flood susceptibility modeling

In this study, the hybridization of SVR and three metaheuristic algorithms of BA, IWO (Mehrabian and Lucas, 2006), and FA (Yang, 2009) were used for flood susceptibility modelling. The BA, IWO, and FA were used to optimize the parameters of SVR to obtain the optimized SVR model. The FR method was also employed to evaluate the effect of each flood conditioning factor on flood occurrences. FR is a bivariate statistical method for estimating the probability relationship between dependent and independent factors, which is commonly used in modeling of the environmental risks as a geostatistical assessment tool (Ranjgar et al., 2021). The suitability and relative importance of these factors were analyzed using the multi-collinearity test and ReliefF algorithm, respectively.

3.3.1. Multi-collinearity analysis

Multi-collinearity among conditioning factors could cause a reduction in model performance accuracy due to the bias between variables it could lead (Saha et al., 2021). In other words, a multi-collinearity test is necessary to determine the suitability of factors for modelling application. The multi-collinearity analysis is carried out using tolerance and variance inflation factor (VIF), where values of tolerance less than 0.1 and a VIF>10 signify the existence of collinearity among factors (Arabameri et al., 2019).

3.3.2. ReliefF feature selection method

Feature selection is a vital preprocessing stage in data mining applications, especially when feature space has many variables. The Relief-based approaches are the only filter-based methods that are capable of identifying feature dependencies (Urbanowicz et al., 2018). However, the original Relief method is scarcely used nowadays and has been substituted by ReliefF (Kononenko, 1994). The 'F' in ReliefF denotes that the algorithm is the sixth variation of the original algorithm. This variation is the best-known and most-used relief-based algorithm in practice up to date. ReliefF is another algorithm similar to ReliefF that uses intermediate weights to compute the final predictor weights differently from ReliefF. The details of this method can be found in (Robnik-Šikonja and Kononenko, 1997).

3.3.3. Optimization of SVR with metaheuristics algorithms

The values of the SVR parameters have a significant impact on its prediction efficiency (Dodangeh et al., 2020; Panahi et al., 2020). In this study, BA, FA, and IWO were used as metaheuristic algorithms to improve the results of the SVR algorithm and for fine-tuning its parameters. Furthermore, RMSE (Eq. (8)) is used as the objective function that the optimization must minimize.

$$\mathrm{RMSE} = \sqrt{\frac{\sum_{i=1}^{n} (X_{obs} - X_{pred})^2}{n}} \tag{8}$$

where X_{obs} is the target data, X_{pred} is the predicted value resulting from the considered flood susceptibility models. Moreover, n is the total number of training or test datasets. When the final conditions are met with the best output, the optimization process stops. Otherwise, the optimization of the parameters is repeated.

3.4. Validation

3.4.1. Evaluation criteria for flood maps

The reference flood map was generated by manual rectification of the flood map derived from the Copernicus emergency management service. Aiming to do so, the surface water was first omitted from the flood map of the Copernicus emergency management service and then manually refined from noise and artefacts. Five evaluation metrics of the miss alarm rate (P_{MA}), false alarm rate (P_{FA}), total error rate (P_{TE}), overall accuracy (OA), F1 score (F_1), and kappa coefficient (Kap) (see Eq. 9–15), which were calculated based on the reference flood map, were employed to assess the effectiveness of the proposed flood detection method.

$$P_{MA} = \left(\frac{FP}{FP + TN}\right) * 100\% \tag{9}$$

$$P_{FA} = \left(\frac{FN}{FN + TP}\right) * 100\% \tag{10}$$

$$P_{TE} = \left(\frac{FN + FP}{FN + TP + FP + TN}\right) * 100\% \tag{11}$$

$$OA = (100 - P_{TE}) \tag{12}$$

$$F_1 = \left(\frac{2TP}{2TP + FP + FN}\right) * 100\% \tag{13}$$

$$Kap = \frac{OA - P_E}{1 - P_E} \tag{14}$$

$$P_E = \frac{(TP + FP).(TP + FN)}{(TP + TN + FP + FN)^2} + \frac{(FN + TN).(FP + TN)}{(TP + TN + FP + FN)^2} \tag{15}$$

In Eq. 9–15, false-positive (FP) is the number of non-flooded pixels which were wrongly labelled as the flooded pixels and false-negative (FN) denotes the number of flood pixels that were wrongly labelled as non-flooded pixels. Moreover, the number of flooded and flooded pixels which were correctly detected are respectively represented by TP (true positive) and TN (true negative).

3.4.2. Modelling evaluation

The RMSE and the ROC curves were used for the quantitative accuracy assessment of the FS models. Considering the binary pattern of the input modelling data (0 = non-flooded, 1 = flooded), the RMSE was calculated using Eq. (8).

The area under the ROC curve (AUROC) is also a typical tool for evaluating the performance and prediction power of models (Farhangi et al., 2020; Razavi-Termeh et al., 2020). AUROC values range from 0 to 1, where the higher values represent more reliable and accurate model performance. The qualitative relationship between AUROC and prediction accuracy of the model can be categorized as follows: 0.5–0.6 (poor), 0.6–0.7 (moderate), 0.7–0.8 (good), 0.8–0.9 (very good), and 0.9–1 (excellent) (Ranjgar et al., 2021; Shogrkhodaei et al., 2021).

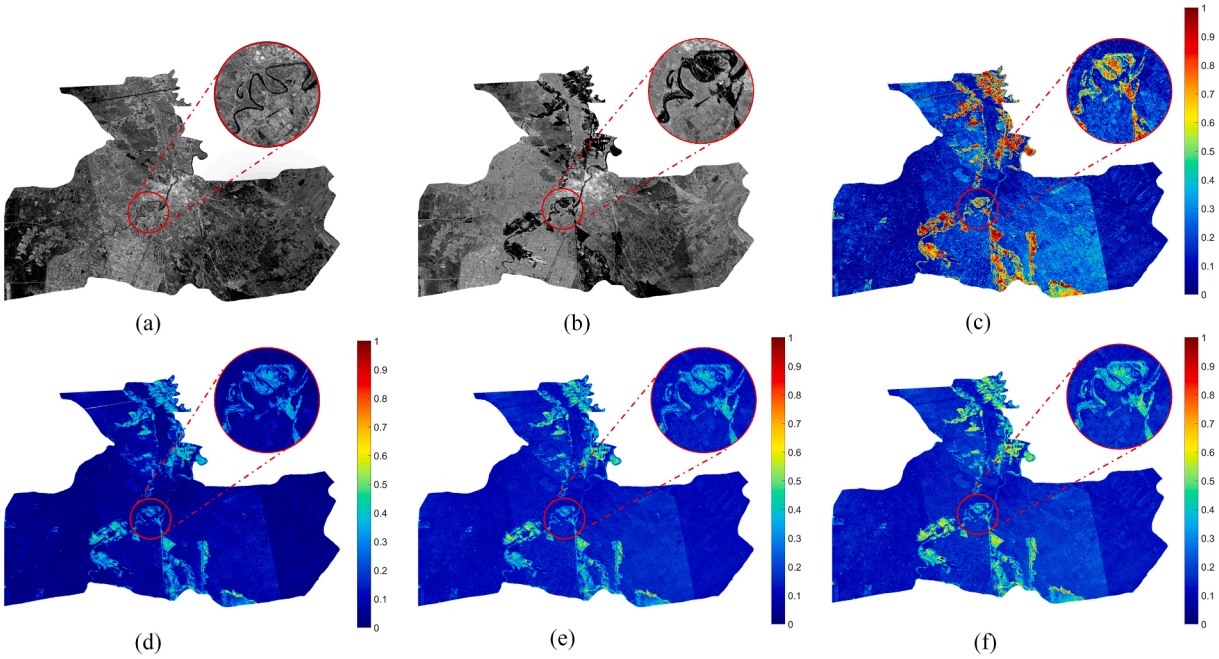

Fig. 5. Bitemporal mosaiced SAR images from Ahwaz, and difference images generated from different methods: Mosaiced Sentinel-1 images acquired on (a) March 11, 2019 and March 24, 2019 (b) April 7, 2019 and April 16, 2019, (c) mean-ratio difference image, (d) log-ratio difference image, (e) normalized difference flood index, and (f) proposed method.

4. Results

4.1. Flood detection results

The visual comparison of the results of the proposed flood detection method, normalized difference flood index, log ratio index, and mean ratio index, (shown in Fig. 5) indicated that the flooded areas in the mean ratio index image were more prominent than those obtained by other methods. Nevertheless, it is dramatically affected by the noise and artefacts, which can result in a high false detection in the final flood map (Fig. 5c). Moreover, although the log ratio index was more robust to anomalies, it missed some parts of the flooded area and did not preserve its geometric details (e.g., boundaries) (Fig. 5d). In contrast, the flooded areas were more prominent in the normalized difference flood index owing to basic insights into the backscattering behavior in its formula. However, the loss of geometrical details of the flooded area is still observed in the results of the normalized difference flood index (Fig. 5e). Overall, the proposed flood detection method, which combines the normalized difference flood index with difference images obtained by the mean ratio index and log ratio index, provided better discrimination between flooded and non-flooded regions (Fig. 5f). For instance, some changed areas that were discarded in the normalized difference flood index and difference images generated by the log ratio index were well highlighted in the results of the proposed method (Fig. 5d-f). This can be mainly due to taking advantage of all mentioned difference images in the form of a single difference image, which boosts the intensity of flood regions while reducing the noise.

The results of the proposed flood detection method were statistically compared with those of the recently proposed flood detection methods (Cian et al., 2018; Moharrami et al., 2021), where the results are provided in Table 1 and Fig. 6. As can be observed from Table 1, the proposed method outperformed the normalized difference flood index and Otsu-based methods considering different accuracy measures. For example, the proposed method could respectively increase the overall accuracy, F score, and Kappa by 0.7 %, 5 %, and 5.51 % compared to the normalized difference flood index. However, the performance of the proposed method on Miss alarm is worse than that of the Otsu-based method. Meanwhile, the Otsu-based method, with an overall accuracy of 91.42 % and a Kappa coefficient of 63.12 achieved the worst accuracy among all methods. In fact, the lack of using the pre-flood image in this method led to recognizing the lakes, rivers, and other smooth surfaces as flood areas and resulted in substantial false alarms.

Table 1
Comparative accuracy results of the flood detection methods.

Method	Miss alarm rate (%)	False alarm rate (%)	Total error rate (%)	Overall accuracy (%)	F1 score	Kappa
Otsu-based	20.96	6.96	8.57	91.42	67.96	63.12
normalized difference flood index	28.65	0.12	3.41	96.59	82.82	80.99
Proposed method	21.52	0.26	2.71	97.29	86.96	85.46

4.2. Flood susceptibility mapping

4.2.1. Multicollinearity test

A multicollinearity test was performed to ensure that the regression assumptions in this study are correct. The VIF and tolerance were implemented to diagnose collinearity in multiple regression and to detect multicollinearity for each flood conditioning factor (see Table 2). It was observed that VIF values for all factors were less than 1.8, indicating that the value of VIF for all independent variables is free of a multicollinearity issue. The VIF score in Table 2 denotes the strength of the correlation between the independent variables. Moreover, the tolerance criterion with values>0.566 indicated satisfying results that confirmed the suitability of all selected flood conditioning factors for further analyses.

4.2.2. Feature selection using the ReliefF method

The results of the ReliefF method, indicating the importance level of the selected flood conditioning factors are shown in Fig. 7. Feature weights (or feature scores) are a type of feature statistic that ranges from

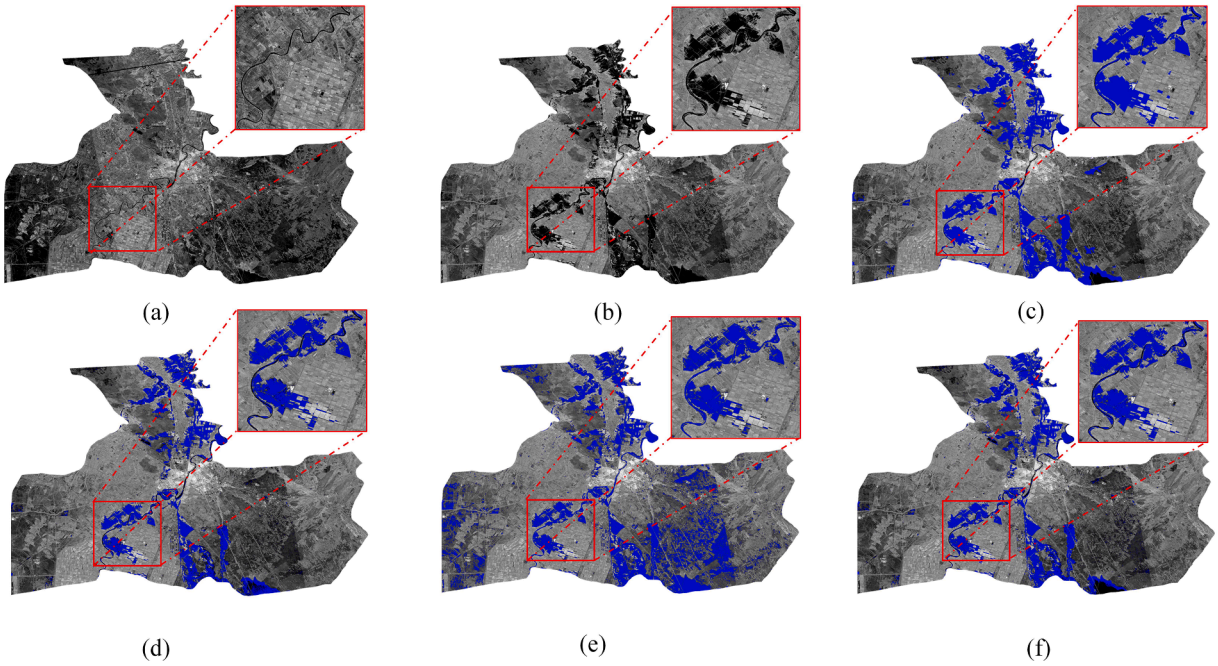

Fig. 6. Detected flood maps using different methods: (a) Pre- and (b) post-mosaiced SAR images captured by sentinel-1 from the city of Ahwaz, (c) reference flood map, flood inundation maps generated by (d) normalized difference flood index (Cian et al., 2018), (e) Otsu-based (Otsu, 1979; Moharrami et al., 2021), and (f) proposed method.

Table 2
Result of multicollinearity analysis.

Flood Conditioning Factor	Tolerance	Variance Inflation Factor (VIF)
Land cover	0.713	1.403
Soil	0.678	1.476
topographic wetness index	0.857	1.167
Rainfall	0.566	1.765
stream power index	0.691	1.448
Curvature	0.842	1.188
Slope	0.588	1.699
Aspect	0.973	1.027
Distance to stream	0.983	1.017
NDVI	0.779	1.284
Altitude	0.770	1.298

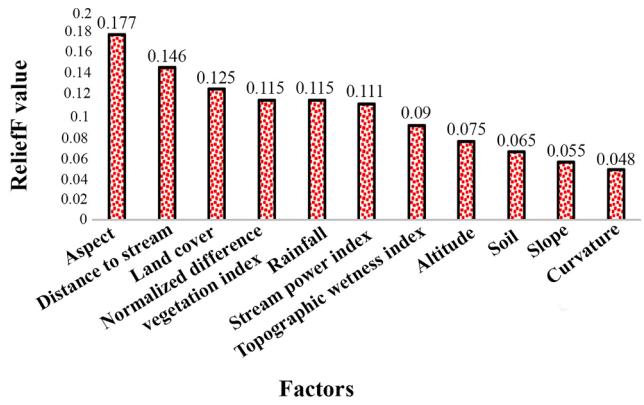

Fig. 7. The importance of flood conditioning factors calculated by the relieff algorithm.

−1 (the worst) to + 1 (the best). The results denoted that all 11 factors were appropriate to predict flood probabilities in this research. In the flood model, the aspect factor was the best predictor, followed by distance to stream, land cover, NDVI, rainfall, topographic wetness index, altitude, soil, slope, and curvature.

4.2.3. Result of FR model

The results of spatial interaction between the flood incidence and the selected flood conditioning factors were obtained using the FR model (see Table 3). On average, FR values greater than one express larger correlations and vice versa (Termeh et al., 2018). The analysis of the FR between flood and altitude indicated that the altitudes of the 24–41 m range had the largest FR values (1.77). All flood occurrences were also in altitudes less than 41 m. As per the distance to stream factor, the highest FR value was in the range of 0–200 m (1.73), and as distance to stream value increased, the FR value declined. Considering the slope factor, more than half of the flood events occurred within the range of 0–1.8 degrees with an FR value of 1.13. The NDVI with the least values (within the range of −0.6- −0.11) has the highest FR value of 2.25. The topographic wetness index class within the 12.75–16 range showed an FR value of 1.42 as the maximum correlation. Also, by the increment of topographic wetness index values, the FR values has increased. Regarding the stream power index, the values belonging to the 20–40 class showed the largest FR. Furthermore, floods occurrences showed drastic drops by the increase of the stream power index values. According to the rainfall factor, the highest (9.52) and lowest values of FR (0.42) was seen in the > 259.7 mm and less than 163.86 mm classes, respectively. Regarding the land lover factor, farmlands and vegetation experienced the largest (105) and the smallest (1) number of floods, respectively, and water body class had the highest FR. According to the soil factor, most floods occurred in the Entisols/Aridisols class, while Inceptisols had the highest FR value (3.07). In the case of the aspect factor, an almost equal distribution of floods was observed in different directions, and the *N* class had the highest FR value (1.29).

4.2.4. Flood susceptibility mapping using hybrid algorithms

The locations of the flooded points needed for modelling were selected from both historical points and the flood detected areas obtained from the proposed RS-based method. In total, 300 flood and 300 non-flood points were selected. For each flood and non-flood group, 70 % of the data (210 points) was randomly used for the modelling

Table 3
Spatial relationship between flood conditioning factors and flood locations using the FR method.

FR	No. of floods	No. pixels in domain	Class	FR	No. of floods	No. pixels in domain	Class
Altitude (m)				Distance to stream (m)			
less than 14	9,975,573	99	0.94	0–200	1,471,439	69	1.73
14–24	5,220,516	42	0.76	200–400	1,274,237	34	0.99
24–41	3,668,543	69	1.77	400–600	1,141,531	32	1.03
41–74	738,652	0	0	600–800	947,560	22	0.86
> 74	207,180	0	0	>800	2,917,671	53	0.67
Slope				NDVI			2.25
0–1.81	9,272,782	111	1.13	−0.6- −0.11	207,631	5	0.82
1.81–3.85	6,745,367	75	1.05	−0.11–0.13	10,788,433	95	1.1
3.58–7.02	2,908,126	24	0.78	0.13–0.27	4,500,050	53	1.3
7.02–12.69	769,535	0	0	0.27–0.47	2,579,399	36	1.27
> 12.69	114,654	0	0	>0.47	1,549,781	21	
Topographic wetness index				Stream power index		120	
less than9.46				0–20	10,544,429	44	1.07
9.46–10.07	5,755,148	50	0.82	20–40	3,315,203	25	1.25
10.07–12.75	6,294,206	62	0.93	400–60	2,106,095	9	1.12
12.75–16	4,022,116	42	0.99	60–80	1,177,927	12	0.72
>16	3,732,539	56	1.42	>80	2,666,809		0.42
	6455	0	0				
Curvature				Rainfall (mm)			
<-1.6	355,169	1	0.27	less than 163.86	1,824,640	21	0.42
−1.6- −0.59	1,785,610	13	0.69	163.86–193.12	1,286,417	52	1.49
−0.59–0.17	9,993,942	115	1.09	193.12–220.2	1,804,262	28	0.57
0.17–1.18	7,062,406	80	1.07	220.2–259.7	2,720,738	79	1.07
>1.18	613,337	1	0.15	>259.7	116,381	30	9.52
Land cover				Soil			
Urban	1,143,039	8	0.58	Inceptisols	443,507	37	3.07
Water body	876,569	22	2.08	Dune Lands	422,147	1	0.09
Wetland	583,025	7	1.00	Entisols/Aridisols	6,215,480	159	0.94
Bare land	9,513,879	67	0.58	Marsh	359,018	12	1.23
Farmland	5,165,958	105	1.69	Bad Lands	294,768	1	0.12
Vegetation	159,898	1	0.52				
aspect							
F	1,449,919	18	1.17				
N	2,409,629	33	1.29				
NE	2,051,799	24	1.10				
E	2,569,698	17	0.62				
SE	2,065,918	17	0.78				
S	2,434,496	24	0.93				
SW	2,114,456	22	0.98				
W	2,639,218	30	1.07				
NW	2,075,331	25	1.14				

(training) procedure and 30 % (90 points) was used for the validation. The spatial distribution of the flood and non-flood locations is shown in Fig. 8.

After normalizing the weights derived from the FR model and assigning them to the factor classes, all the input locations and their corresponding values of flood conditioning factors were imported into the MATLAB R2017b software. According to the RMSE results of the training and validation samples shown in Table 4, SVR-FA with the RMSE values of 0.3058 and 0.3538 (for training and validation, respectively) outperformed the other algorithms, followed by SVR-IWO (0.3177, 0.3742), SVR-BA (0.333, 0.3783), and SVR (0.3602, 0.3952), respectively. The optimum parameters of the SVR, including C, $\in$ and γ, were also calculated by setting an iteration process in each hybrid algorithm based on minimizing the RMSE value as the optimization criterion. The optimized parameters of the SVR-BA, SVR-IWO, and SVR-FA hybrid algorithms are also provided in Table 4.

The target and output values of the employed models for all flood samples are shown in Fig. 9 to display the levels of prediction error. According to Fig. 9a, the difference between the targets and outputs in the SVR model was considerably greater than those of the hybrid methods. This result is even worse in the case of validation samples, indicating that the optimization algorithms could significantly improve the SVR performance. The highest overall accuracy of the 420 training samples was obtained by the SVR-FA model, while the non-optimized version of SVR denoted the least level of correlation for the validation samples.

After conducting SVR hybrid modelling with metaheuristics, the outputs were transferred into the ArcGIS 10.3 software to produce the simulation results of the proposed hybrid methods. Based on the natural break classifier, the classified flood susceptibility maps were divided into five susceptibility classes of very low, low, medium, high, and very high susceptibility levels (Termeh et al., 2018). Based on the results demonstrated in Fig. 10, all investigated models showed almost similar susceptibility maps (e.g., approximately similar extent and spatial distribution of susceptibility classes).

The extent percentages of flood susceptibility classes obtained from the proposed models were summarized in Table 5. Compared to the other models, the SVR allocated a smaller number of pixels to the very low susceptibility class while showing the largest extent of low susceptible areas (with 39 %). The SVR-FA, as the more accurate model, indicated that the susceptibility classes of very low, low, moderate, high, and very high roughly corresponded to 12 %, 36 %, 31 %, 17 %, and 3 % of the study area. The percentages of such susceptibility classes for SVR-BA were 18 %, 38 %, 27 %, 15 %, and 2 %, respectively. Similarly, the corresponding percentages of SVR-IWO were 18 %, 31 %, 30 %, 17 %, and 4 %, respectively. Considering all models, almost a fifth of the entire study area was prone to high and very high flood susceptible classes.

4.2.5. *Validation of flood susceptibility maps*

In general, AUROC values of>0.5 are usually known as the suitable

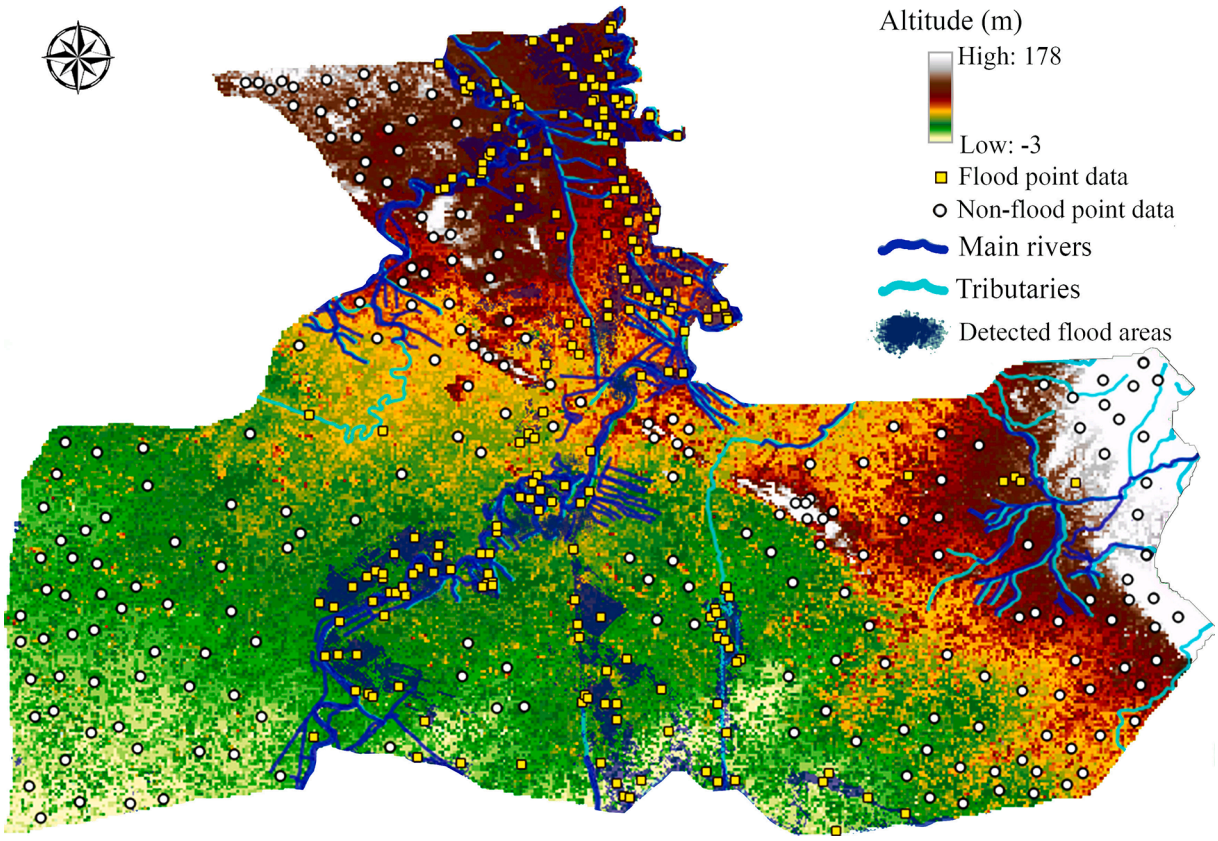

Fig. 8. The flood inventory map from the study area along with the spatial distribution of the flood and non-flood points used for model training and validation, respectively.

Table 4
RMSE results of the training and validation data, and the optimized parameters of the hybrid models.

Model	Training	Validation	Optimized parameters
SVR	0.3602	0.3952	–
SVR-BA	0.333	0.3783	C = 6.99, ∈= 0.323, γ = 5.54
SVR-IWO	0.3177	0.3742	C = 1.77, ∈= 0.303, γ = 6.36
SVR-FA	0.3058	0.3538	C = 10.62, ∈= 0.264, γ = 8.88

range for validation purposes. According to the ROC curves (Fig. 11) and AUROC results (Table 6), all models indicated satisfying sensitivity results (with AUROC values > 0.77), implying the fact that these models were appropriate for flood susceptibility analyses. The predictive power of the SVR-FA was the highest with the AUROC value of 0.806, which was followed by SVR-IWO, SVR-BA, and SVR with the values of 0.802, 0.793, and 0.774, respectively. This indicated the high predictive performance of all three hybrid models compared to the standalone SVR.

5. Discussion

5.1. Impact of flood conditioning factors on flood

The importance analysis of the flood-related variables, derived from the ReliefF method, showed that the aspect, distance to stream, and land cover conditioning factors were respectively the most significant variables that contributed to the flood occurrence. This is almost in contrast with the results reported by Hong et al. (2018) and (Razavi Termeh et al., 2018). The most important flood conditioning factors in the study conducted by Hong et al. (2018) were altitude, topographic wetness index, and distance from the river. (Razavi Termeh et al., 2018) also reported that the slope, rainfall, and altitude were the most important factors contributing to the floods in their case study. The reason why the aspect was more important in this study could be due to its indirect effect on the surface runoff through its impact on other factors like rainfall regime, soil humidity, and solar radiation. The aspect showed that the largest extent of the study area was along the south direction followed by south-east and south-west. This is consistent with results reported by Regmi et al. (2014). Distance to stream is of high importance because those regions that are closer to streams and main rivers are obviously more prone to inundations and runoffs. The significant role of distance to stream in flood occurrence has frequently been addressed in the literature, i.e., (Danumah et al., 2016; Gigović et al., 2017). The significance of land cover is because the land cover of an area determines its water infiltration rate. The high contribution of land cover in flood occurrence found in this study could be justifiable since bare lands or scantily vegetated areas have been reported to be more susceptible to flooding due to their low percolation level and high runoff (Talha et al., 2019; Souissi et al., 2020).

As regards the land cover factor (see Table 3), the water body class, farmlands, and wetlands were respectively the most susceptible areas to flooding with the highest FR values. Regarding the land cover map, a large portion of the water body and farmland classes was specifically located in the central northern regions of the study area where two of the main rivers (Dez and Karoun) enter Ahwaz city. This region is where the highly susceptible areas were located in the produced flood susceptibility maps. Larger changes in slope were also observed in such areas. This could be a reason for the water runoff of the mentioned rivers. The noticeable influence of the class of water bodies on flood susceptibility has also been addressed by Paul et al. (2019), and Tella and Balogun, (2020). The farmlands at the river banks were observed at special risk of flood hazards presumably due to the frequent runoff occurrences in the vicinity of the main streams and tributaries. Moreover, the low permeability and limited water infiltration of wetlands have the potential to

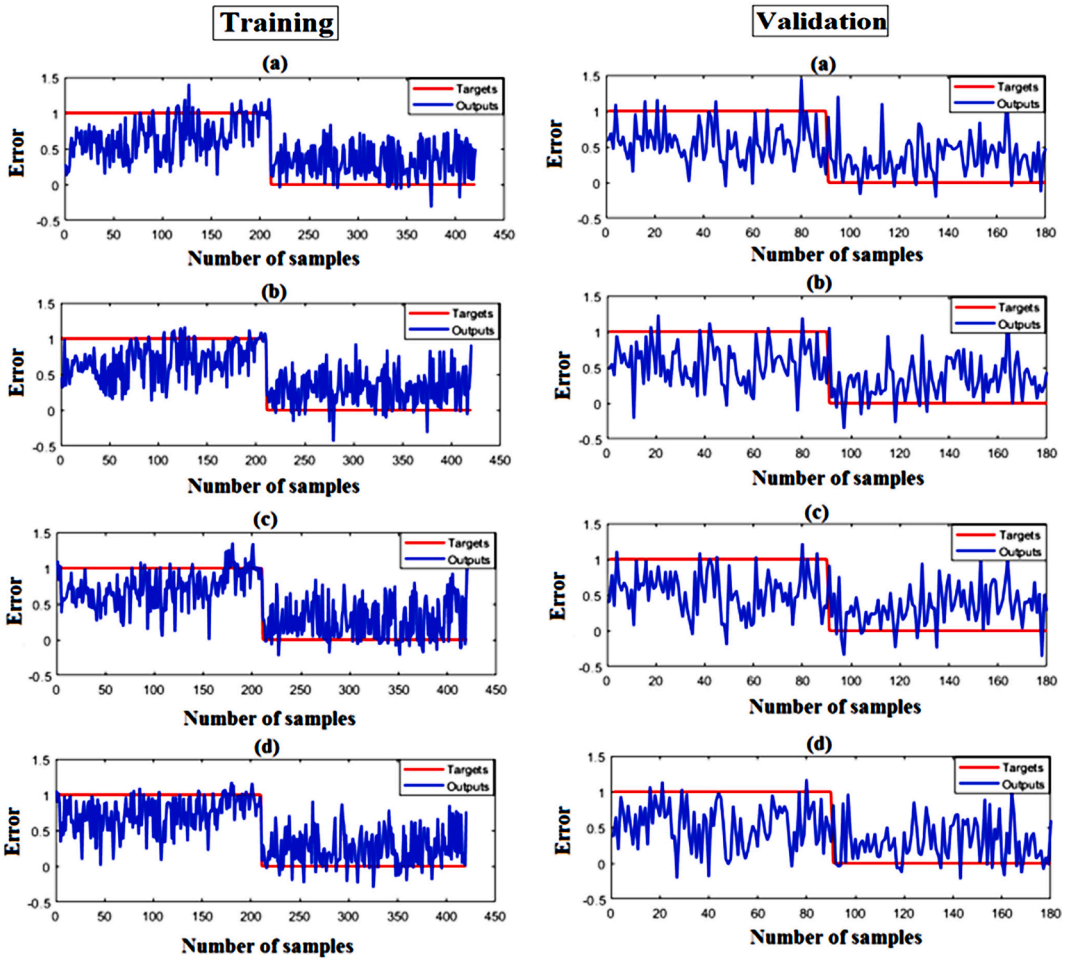

Fig. 9. Results of prediction error obtained from (a) SVR, (b) SVR-BA, (c) SVR-IWO, and (d) SVR-FA.

lead to the maximum water capacity, spillage or overflow after a series of rainfall events, hence floating a large amount of water to downstream areas through surface flows.

As per the altitude factor, the largest FR value was observed for the altitudes less than 24 m, and the low altitudes of the region can be considered as the flood prone-areas. According to Fig. 10, very high susceptible areas of the susceptibility maps can be found in both high and low altitudes. The topographic wetness index indicated that its larger values had the larger FR values. Large values of the topographic wetness index were reported to correspond to the regions that are prone to water accumulation and high runoff, and indicate how low drainage, representing more saturated land, can trigger flash flooding (Swain et al., 2020). The inverse relation between the stream power index and FR values was observed. The stream power index delineates soil water content and erosion power of floods to flow downwards in a watershed, hence some areas with the potential of flow accumulation are indicated by the lower values of the stream power index. This was the reason why most floods in the study area occurred in places with lower values of the stream power index. This inverse relation has also been addressed by Swain et al. (2020). In accordance with the NDVI, values less than −0.11 were found to have higher FR, indicating that regions with low vegetation levels were more flood-prone and vice versa. This relation is also addressed by Bui et al. (2019).

5.2. Analysis of flood maps

Considering the flood maps illustrated in Fig. 6, the maps produced by the Otsu-based method were considerably affected by noise and anomalies where plenty of surface water (or water bodies) were misclassified as flooded areas. This limitation was well addressed by the normalized difference flood index and the proposed approach (Fig. 6c-f). Most of the flooded regions were accurately detected using the normalized difference flood index but with several false alarms compared to the proposed method. Moreover, the geometrical details of the flood areas were more preserved by the proposed method (Fig. 6c, 6f). This is probably due to a combination of change detection and water body detection in its process. Nevertheless, multiple small flooded areas were missed in the maps generated by the normalized difference flood index and the proposed method which can be due to the lack of the contextual information used in the core of these methods (Fig. 6c, 6e and 7f). In this study, the remotely detected flood maps could provide the model input with numerous training points, while traditionally made maps usually suffer from the inadequate spatial distribution of data points. Moreover, since the employed SAR data is not subject to clouds and atmospheric conditions, the proposed method took advantage of multi-temporal consistently available data.

5.3. Comparison of the flood susceptibility models

Based on Figs. 9 and 11, and Table 6, the FA-SVR outperformed the other models, while the non-optimized SVR was found as the weakest model. Although the final flood susceptibility maps of the hybrid models were in line with each other, the standalone SVR was relatively different. The same results were observed for the level of prediction power of the models where the hybrid models showed a close performance (see ROC curves in Fig. 11). However, SVR had the lowest

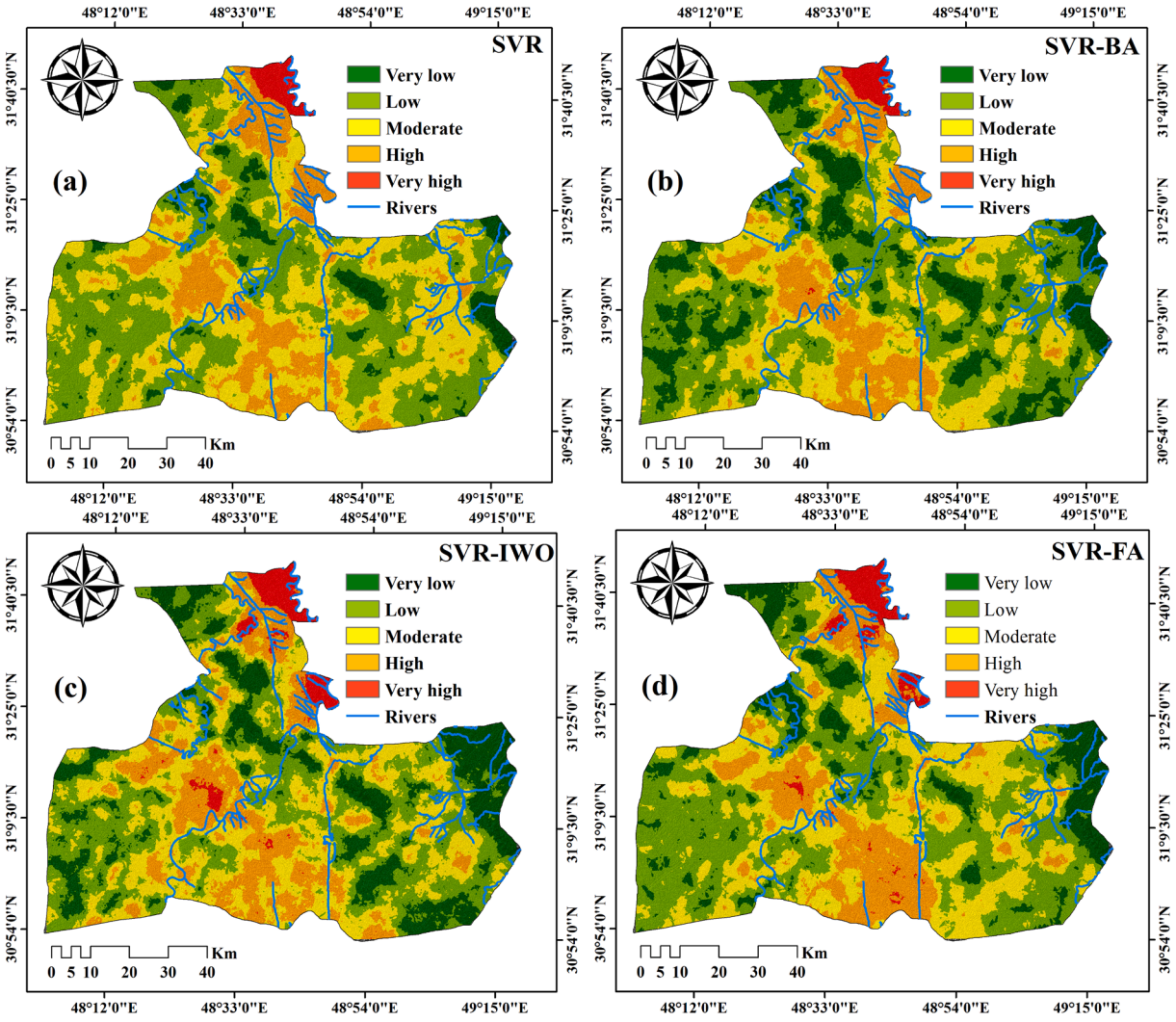

Fig. 10. Flood susceptibility maps produced by: (a) SVR, (b) SVR-BA, (c) SVR-IWO, and (d) SVR-FA.

Table 5
Area percentage of each flood susceptibility class based on different models.

model	Very low	Low	Moderate	High	Very high
SVR	6.48 %	39.19 %	36.57 %	16.1 %	1.66 %
SVR-BA	17.81 %	37.86 %	27.44 %	15.21 %	1.68 %
SVR-IWO	17.65 %	31.45 %	29.89 %	17.44 %	3.57 %
SVR-FA	12.31 %	36.35 %	30.81 %	17.22 %	3.31 %

accuracy in predicting the same pattern. The efficiency of the employed *meta*-heuristic algorithms for optimization of the flood susceptibility maps has been addressed by Khosravi et al. (2018a,b), which is consistent with the results of this study. The better predictive power of the hybridized SVR models using *meta*-heuristic algorithms was also approved by (Pourghasemi et al., 2020) which was in line with the results of this study. Aiming at spatial modelling of urban flood inundation, the efficiency of some hybridized (integrated with a configuration of the wavelet transform, grey wolf optimizer and bat optimizer) and standalone SVR models was evaluated by Rahmati et al. (2020). Their results showed the superiority of the hybridized SVR against the standalone SVR models. Generally, the high efficiency of hybridized SVR models, as a solution to linear and non-linear problems, has been reported for many practical problems, especially flood susceptibility modelling (Saha et al., 2021; Siam et al., 2021). Many ensemble models that combine several single statistical or machine learning methods have

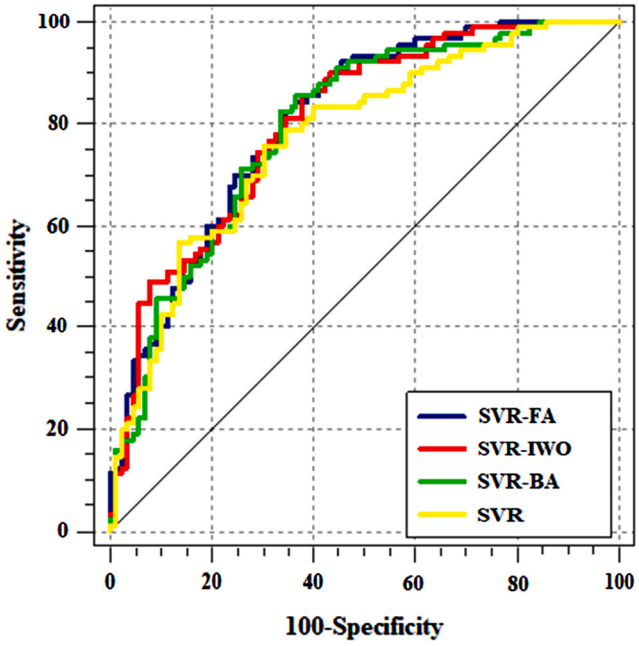

Fig. 11. Result of ROC curves of the hybrid models.

Table 6
The results of the area under the ROC curve (AUROC) related to the flood susceptibility models.

Models	AUROC	Standard error	Asymptotic 95 % confidence interval	
			Lower bound	Upper bound
SVR-FA	0.806	0.0319	0.741	0.861
SVRIWO	0.802	0.0323	0.737	0.858
SVR-BA	0.793	0.0334	0.727	0.850
SVR	0.774	0.0346	0.705	0.833

proved effective in improving the flood mapping results (i.e., (Shafizadeh-Moghadam et al., 2018; Islam et al., 2021).

In this study, the FA, IWO, and BA algorithms had the highest accuracy in optimizing the SVR model, respectively. Auto-segmentation and the ability to handle a multi-quality challenge are two of the FA algorithm's main advantages. With the help of the FA algorithm, the total population will be divided into subgroups with a mean interval, and each group will be able to conquer an optimal location. This division makes it possible to find the best one at a time. Unlike other *meta*-heuristic algorithms, the IWO permits all potential candidates to participate in the reproduction process. One of the disadvantages of the IWO algorithm is the increase of computational time and convergence to local optimization (Ahmadi and Mojallali, 2012). The BA is simple, flexible, and easy to implement, but this algorithm converges very quickly in the early stages and then slows down. There is also no mathematical analysis for the relationship between the parameters and the convergence rate. Therefore, in this study, this algorithm was less accurate than the other two algorithms.

5.4. Comparison, limitation, and future work

Several approaches have so far been used for flood susceptibility mapping, among of which the methods depending on the geomorphologic characteristics of a basin have frequently been employed in many studies (Nardi et al., 2006; Degiorgis et al., 2012; Samela et al., 2018). Although hydrogeomorphic methods extensively use DEMs and terrain analysis for preliminary floodplains characterizations, accurate inundation/flood mapping is generally based on advanced hydrologic and hydraulic modelling (Grimaldi et al., 2013; Ezzine et al., 2020). These methods cannot replace hydrology and hydraulic modelling which are based on actual physical processes (Vojtek and Vojteková, 2019).

The conventional hydrologic and hydraulic modeling approaches need various types of resources to collect the required data and run the models after appropriate calibration and validation. In this regard, some of the important data consist of DEM, soil, land use, river bathymetry, hydrological data, and details of man-made structures along the intended reach. This approach is commonly employed to create flood maps for individual river segments where such data is available or can be acquired through resources. On the other hand, flood maps generated through modeling can suffer from high level of uncertainty in data-scarce areas (Jafarzadegan and Merwade, 2017). Although the hydrologic and hydraulic modeling approach should always be the first priority for inundation/flood mapping efforts, the proposed method of this study could be employed as an alternate approach when the required data is limited or unavailable, especially in large-scale analysis or in developing countries. A notable limitation of the proposed flood detection method could be the limited temporal resolution of satellite imagery, because it can lead to missing the flood extent map at its peak time. Moreover, another limitation of the proposed susceptibility mapping method is that it highly relies on the quality and precision of the flood conditioning factors which are usually provided from diverse sources.

In large-scale flood susceptibility mapping tasks, finding the optimal balance between the flood susceptibility model complexity and the accuracy and amount of the input data is generally challenging. Aiming to address this issue, future studies can deal with the challenges related to data consolidation, especially by improving their original scale, resolution, or generalization. Moreover, RS data can be applied to hydrological and hydraulic modelling through three different scenarios: (1) model input integration by providing information on the basin or boundary conditions; (2) model calibration or parameter estimation; and (3) data assimilation (Xu et al., 2014). Future studies can investigate novel capability integrations of hydrological modelling, RS, GIS and geomorphology to provide accurate inferences about the dynamics of flooded areas and flood-prone regions.

6. Conclusion

Flood is one of the most catastrophic phenomena in the world and is a drastic danger to many aspects of life. Aiming to mitigate human losses and flood damage, producing a flood hazard susceptibility map is an important step in any flood management plan. One challenge of susceptibility map generations in many countries is the lack of adequate and up-to-date field data to be used for the training step of machine learning methods. Moreover, flood susceptibility map production is generally subject to two main components, pace and accuracy. In this study, a combination of RS, GEE, and GIS capabilities were used to produce the required speed and accuracy in susceptibility map generations. In this regard, a novel RS-based flood detection method along with three hybridized SVR models was developed to automatically and quickly produce susceptibility maps. The RMSE results of the training and validation samples used in this study indicated that the SVR-FA could outperform the other models. The evaluation of the prediction power of all models also showed that the SVR-FA was superior with a larger AUROC value. In general, the weakest model was the standalone SVR model, which indicates the efficient impact of using the optimum SVR parameters on modelling. The flood susceptibility map results showed that the northern areas of Ahwaz, where a couple of main rivers and tributaries come together, were the most vulnerable regions, and farmlands were the high-risk regions. The produced flood susceptibility maps of this study can help the governors and planners, water resources organizations, environment-related organizations, and natural resource managers to take proper actions for flood damage reductions.

Funding sources

This research did not receive any specific grant from funding agencies in the public, commercial, or not-for-profit sectors.

CRediT authorship contribution statement

Soroosh Mehravar: Conceptualization, Methodology, Validation, Writing – original draft, Visualization, Data curation, Formal analysis. **Seyed Vahid Razavi-Termeh:** Conceptualization, Methodology, Writing – review & editing, Data curation. **Armin Moghimi:** Conceptualization, Methodology, Validation, Data curation, Visualization, Writing – original draft. **Babak Ranjgar:** Methodology, Writing – original draft, Formal analysis, Investigation. **Fatemeh Foroughnia:** Formal analysis, Investigation, Writing – review & editing. **Meisam Amani:** Writing – review & editing, Supervision.

Declaration of Competing Interest

The authors declare that they have no known competing financial interests or personal relationships that could have appeared to influence the work reported in this paper.

Data availability

Data will be made available on request.

Appendix A. Supplementary data

Supplementary data to this article can be found online at https://doi.org/10.1016/j.jhydrol.2023.129100.

References

Ahmadi, M., Mojallali, H., 2012. Chaotic invasive weed optimization algorithm with application to parameter estimation of chaotic systems. Chaos, Solitons & Fractals 45, 1108–1120.

Al-Juaidi, A.E.M., Nassar, A.M., Al-Juaidi, O.E.M., 2018. Evaluation of flood susceptibility mapping using logistic regression and GIS conditioning factors. Arab. J. Geosci. 11, 1–10.

Ansari, M., Akhoondzadeh, M., 2020. Mapping water salinity using Landsat-8 OLI satellite images (Case study: Karun basin located in Iran). Adv. Sp. Res. 65, 1490–1502.

Arabameri, A., Rezaei, K., Cerdà, A., Conoscenti, C., Kalantari, Z., 2019. A comparison of statistical methods and multi-criteria decision making to map flood hazard susceptibility in Northern Iran. Sci. Total Environ. 660, 443–458.

Arora, A., Arabameri, A., Pandey, M., Siddiqui, M.A., Shukla, U.K., Bui, D.T., Mishra, V. N., Bhardwaj, A., 2021. Optimization of state-of-the-art fuzzy-metaheuristic ANFIS-based machine learning models for flood susceptibility prediction mapping in the Middle Ganga Plain. India. Sci. Total Environ. 750, 141565.

Balogun, A.-L., Rezaie, F., Pham, Q.B., Gigović, L., Drobnjak, S., Aina, Y.A., Panahi, M., Yekeen, S.T., Lee, S., 2021. Spatial prediction of landslide susceptibility in western Serbia using hybrid support vector regression (SVR) with GWO. BAT and COA algorithms. Geosci. Front. 12, 101104.

Bui, D.T., Pradhan, B., Nampak, H., Bui, Q.-T., Tran, Q.-A., Nguyen, Q.-P., 2016. Hybrid artificial intelligence approach based on neural fuzzy inference model and metaheuristic optimization for flood susceptibilitgy modeling in a high-frequency tropical cyclone area using GIS. J. Hydrol. 540, 317–330.

Bui, D.T., Ngo, P.-T.-T., Pham, T.D., Jaafari, A., Minh, N.Q., Hoa, P.V., Samui, P., 2019. A novel hybrid approach based on a swarm intelligence optimized extreme learning machine for flash flood susceptibility mapping. Catena 179, 184–196.

Cao, C., Xu, P., Wang, Y., Chen, J., Zheng, L., Niu, C., 2016. Flash flood hazard susceptibility mapping using frequency ratio and statistical index methods in coalmine subsidence areas. Sustainability 8, 948.

Chapi, K., Singh, V.P., Shirzadi, A., Shahabi, H., Bui, D.T., Pham, B.T., Khosravi, K., 2017. A novel hybrid artificial intelligence approach for flood susceptibility assessment. Environ. Model. Softw. 95, 229–245.

Choubin, B., Moradi, E., Golshan, M., Adamowski, J., Sajedi-Hosseini, F., Mosavi, A., 2019. An ensemble prediction of flood susceptibility using multivariate discriminant analysis, classification and regression trees, and support vector machines. Sci. Total Environ. 651, 2087–2096.

Cian, F., Marconcini, M., Ceccato, P., 2018. Normalized Difference Flood Index for rapid flood mapping: Taking advantage of EO big data. Remote Sens. Environ. 209, 712–730.

Danumah, J.H., Odai, S.N., Saley, B.M., Szarzynski, J., Thiel, M., Kwaku, A., Kouame, F. K., Akpa, L.Y., 2016. Flood risk assessment and mapping in Abidjan district using multi-criteria analysis (AHP) model and geoinformation techniques,(cote d'ivoire). Geoenvironmental Disasters 3, 1–13.

de Brito, M.M., Almoradie, A., Evers, M., 2019. Spatially-explicit sensitivity and uncertainty analysis in a MCDA-based flood vulnerability model. Int. J. Geogr. Inf. Sci. 33, 1788–1806.

de Moel, H., Jongman, B., Kreibich, H., Merz, B., Penning-Rowsell, E., Ward, P.J., 2015. Flood risk assessments at different spatial scales. Mitig. Adapt. Strateg. Glob. Chang. 20, 865–890.

Degiorgis, M., Gnecco, G., Gorni, S., Roth, G., Sanguineti, M., Taramasso, A.C., 2012. Classifiers for the detection of flood-prone areas using remote sensed elevation data. J. Hydrol. 470, 302–315.

Dineva, A., Várkonyi-Kóczy, A.R., Tar, J.K., 2014. Fuzzy expert system for automatic wavelet shrinkage procedure selection for noise suppression, in: IEEE 18th International Conference on Intelligent Engineering Systems INES 2014. IEEE, pp. 163–168.

Dodangeh, E., Panahi, M., Rezaie, F., Lee, S., Bui, D.T., Lee, C.-W., Pradhan, B., 2020. Novel hybrid intelligence models for flood-susceptibility prediction: Meta optimization of the GMDH and SVR models with the genetic algorithm and harmony search. J. Hydrol. 590, 125423.

Ezzine, A., Saidi, S., Hermassi, T., Kammessi, I., Darragi, F., Rajhi, H., 2020. Flood mapping using hydraulic modeling and Sentinel-1 image: Case study of Medjerda Basin, northern Tunisia. Egypt. J. Remote Sens. Sp. Sci. 23, 303–310.

Falah, F., Rahmati, O., Rostami, M., Ahmadisharaf, E., Daliakopoulos, I.N., Pourghasemi, H.R., 2019. Artificial neural networks for flood susceptibility mapping in data-scarce urban areas, in: Spatial Modeling in GIS and R for Earth and Environmental Sciences. Elsevier, pp. 323–336.

Farhangi, F., Sadeghi-Niaraki, A., Nahvi, A., Razavi-Termeh, S.V., 2020. Spatial modeling of accidents risk caused by driver drowsiness with data mining algorithms. Geocarto Int. 1–15.

Ghorbanian, A., Kakooei, M., Amani, M., Mahdavi, S., Mohammadzadeh, A., Hasanlou, M., 2020. Improved land cover map of Iran using Sentinel imagery within Google Earth Engine and a novel automatic workflow for land cover classification using migrated training samples. ISPRS J. Photogramm. Remote Sens. 167, 276–288. https://doi.org/10.1016/J.ISPRSJPRS.2020.07.013.

Gigović, L., Pamučar, D., Bajić, Z., Drobnjak, S., 2017. Application of GIS-interval rough AHP methodology for flood hazard mapping in urban areas. Water 9, 360.

Grimaldi, S., Petroselli, A., Arcangeletti, E., Nardi, F., 2013. Flood mapping in ungauged basins using fully continuous hydrologic–hydraulic modeling. J. Hydrol. 487, 39–47.

Hong, W.-C., 2008. Rainfall forecasting by technological machine learning models. Appl. Math. Comput. 200, 41–57.

Hong, H., Tsangaratos, P., Ilia, I., Liu, J., Zhu, A.-X., Chen, W., 2018. Application of fuzzy weight of evidence and data mining techniques in construction of flood susceptibility map of Poyang County. China. Sci. Total Environ. 625, 575–588.

Islam, A.R.M.T., Talukdar, S., Mahato, S., Kundu, S., Eibek, K.U., Pham, Q.B., Kuriqi, A., Linh, N.T.T., 2021. Flood susceptibility modelling using advanced ensemble machine learning models. Geosci. Front. 12, 101075.

Jafarzadegan, K., Merwade, V., 2017. A DEM-based approach for large-scale floodplain mapping in ungauged watersheds. J. Hydrol. 550, 650–662.

Janizadeh, S., Avand, M., Jaafari, A., Phong, T.V., Bayat, M., Ahmadisharaf, E., Prakash, I., Pham, B.T., Lee, S., 2019. Prediction success of machine learning methods for flash flood susceptibility mapping in the tafresh watershed. Iran. Sustainability 11, 5426.

Kalantar, B., Ueda, N., Saeidi, V., Janizadeh, S., Shabani, F., Ahmadi, K., Shabani, F., 2021. Deep neural network utilizing remote sensing datasets for flood hazard susceptibility mapping in Brisbane. Australia. Remote Sens. 13, 2638.

Khosravi, K., Panahi, M., Bui, D.T., 2018a. A comprehensive study of new hybrid models for Adaptive Neuro-Fuzzy Inference System (ANFIS) with Invasive Weed Optimization (IWO). 2 Differential Evolution (DE), Firefly (FA), Particle Swarm Optimization (PSO) 3 and Bees (BA) Algorithms for Spatial Predi.

Khosravi, K., Panahi, M., Tien Bui, D., 2018b. Spatial prediction of groundwater spring potential mapping based on an adaptive neuro-fuzzy inference system and metaheuristic optimization. Hydrol. Earth Syst. Sci. 22, 4771–4792.

Khosravi, K., Melesse, A.M., Shahabi, H., Shirzadi, A., Chapi, K., Hong, H., 2019a. Flood susceptibility mapping at Ningdu catchment, China using bivariate and data mining techniques. Extreme Hydrology and Climate Variability. Elsevier 419–434.

Khosravi, K., Shahabi, H., Pham, B.T., Adamowski, J., Shirzadi, A., Pradhan, B., Dou, J., Ly, H.-B., Gróf, G., Ho, H.L., 2019b. A comparative assessment of flood susceptibility modeling using multi-criteria decision-making analysis and machine learning methods. J. Hydrol. 573, 311–323.

Kim, S., Matsumi, Y., Pan, S., Mase, H., 2016. A real-time forecast model using artificial neural network for after-runner storm surges on the Tottori coast. Japan. Ocean Eng. 122, 44–53.

Kononenko, I., 1994. Estimating attributes: Analysis and extensions of RELIEF. European Conference on Machine Learning. Springer 171–182.

Liu, J., Xiong, J., Cheng, W., Li, Y., Cao, Y., He, Y., Duan, Y., He, W., Yang, G., 2021. Assessment of Flood Susceptibility Using Support Vector Machine in the Belt and Road Region. Nat. Hazards Earth Syst. Sci. Discuss. 1–37.

J. MacQueen Some methods for classification and analysis of multivariate observations 1967 Oakland, CA, USA 281 297.

Mahdavi, S., Salehi, B., Huang, W., Amani, M., Brisco, B., 2019. A PolSAR change detection index based on neighborhood information for flood mapping. Remote Sens. 11, 1854.

Martinis, S., Plank, S., Ćwik, K., 2018. The use of Sentinel-1 time-series data to improve flood monitoring in arid areas. Remote Sens. 10 https://doi.org/10.3390/rs10040583.

Mehrabian, A.R., Lucas, C., 2006. A novel numerical optimization algorithm inspired from weed colonization. Ecol. Inform. 1, 355–366.

Mehravar, S., Amani, M., Moghimi, A., Javan, F.D., Samadzadegan, F., Ghorbanian, A., Stein, A., Mohammadzadeh, A., Mirmazloumi, S.M., 2021. Temperature-Vegetation-soil Moisture-Precipitation Drought Index (TVMPDI); 21-year drought monitoring in Iran using satellite imagery within Google Earth Engine. Adv. Sp. Res.

Moghimi, A., Khazai, S., Mohammadzadeh, A., 2017a. An improved fast level set method initialized with a combination of k-means clustering and Otsu thresholding for unsupervised change detection from SAR images. Arab. J. Geosci. 10, 1–18. https://doi.org/10.1007/s12517-017-3072-3.

Moghimi, A., Mohammadzadeh, A., Khazai, S., 2017b. Integrating Thresholding With Level Set Method for Unsupervised Change Detection in Multitemporal SAR Images. Can. J. Remote Sens. 43, 412–431. https://doi.org/10.1080/07038992.2017.1342205.

Moharrami, M., Javanbakht, M., Attarchi, S., 2021. Automatic flood detection using sentinel-1 images on the google earth engine. Environ. Monit. Assess. 193, 1–17.

Mosavi, A., Ozturk, P., Chau, K., 2018. Flood prediction using machine learning models: Literature review. Water 10, 1536.

Nardi, F., Vivoni, E.R., Grimaldi, S., 2006. Investigating a floodplain scaling relation using a hydrogeomorphic delineation method. Water Resour. Res. 42.

Ngo, P.-T.-T., Pham, T.D., Nhu, V.-H., Le, T.T., Tran, D.A., Phan, D.C., Hoa, P.V., Amaro-Mellado, J.L., Bui, D.T., 2021. A novel hybrid quantum-PSO and credal decision tree ensemble for tropical cyclone induced flash flood susceptibility mapping with geospatial data. J. Hydrol. 596, 125682.

Otsu, N., 1979. THRESHOLD SELECTION METHOD FROM GRAY-LEVEL HISTOGRAMS. IEEE Trans Syst Man Cybern. https://doi.org/10.1109/tsmc.1979.4310076.

Panahi, M., Gayen, A., Pourghasemi, H.R., Rezaie, F., Lee, S., 2020. Spatial prediction of landslide susceptibility using hybrid support vector regression (SVR) and the adaptive neuro-fuzzy inference system (ANFIS) with various metaheuristic algorithms. Sci. Total Environ. 741, 139937.

Panahi, M., Dodangeh, E., Rezaie, F., Khosravi, K., Van Le, H., Lee, M.-J., Lee, S., Pham, B.T., 2021. Flood spatial prediction modeling using a hybrid of meta-optimization and support vector regression modeling. Catena 199, 105114.

Parsian, S., Amani, M., Moghimi, A., Ghorbanian, A., Mahdavi, S., 2021. Flood Hazard Mapping Using Fuzzy Logic, Analytical Hierarchy Process, and Multi-Source Geospatial Datasets. Remote Sens. 13, 4761.
Paul, G.C., Saha, S., Hembram, T.K., 2019. Application of the GIS-based probabilistic models for mapping the flood susceptibility in Bansloi sub-basin of Ganga-Bhagirathi river and their comparison. Remote Sens. Earth Syst. Sci. 2, 120–146.
Pourghasemi, H.R., Gayen, A., Panahi, M., Rezaie, F., Blaschke, T., 2019. Multi-hazard probability assessment and mapping in Iran. Sci. Total Environ. 692, 556–571.
Pourghasemi, H.R., Razavi-Termeh, S.V., Kariminejad, N., Hong, H., Chen, W., 2020. An assessment of metaheuristic approaches for flood assessment. J. Hydrol. 582, 124536.
Rahmati, O., Pourghasemi, H.R., Zeinivand, H., 2016a. Flood susceptibility mapping using frequency ratio and weights-of-evidence models in the Golastan Province. Iran. Geocarto Int. 31, 42–70.
Rahmati, O., Zeinivand, H., Besharat, M., 2016b. Flood hazard zoning in Yasooj region, Iran, using GIS and multi-criteria decision analysis. Geomatics. Nat. Hazards Risk 7, 1000–1017.
Rahmati, O., Darabi, H., Panahi, M., Kalantari, Z., Naghibi, S.A., Ferreira, C.S.S., Kornejady, A., Karimidastenaei, Z., Mohammadi, F., Stefanidis, S., 2020. Development of novel hybridized models for urban flood susceptibility mapping. Sci. Rep. 10, 1–19.
Ranjgar, B., Razavi-Termeh, S.V., Foroughnia, F., Sadeghi-Niaraki, A., Perissin, D., 2021. Land subsidence susceptibility mapping using persistent scatterer SAR interferometry technique and optimized hybrid machine learning algorithms. Remote Sens. 13, 1326.
Razavi Termeh, S.V., Pourghasemi, H.R., Alidadganfard, F., 2018. Flood inundation susceptibility mapping using analytical hierarchy process (AHP) and TOPSIS decision making methods and weight of evidence statistical model (case study: jahrom township, fars province). J. watershed Manag. Res. 9, 67–81.
Razavi-Termeh, S.V., Khosravi, K., Sadeghi-Niaraki, A., Choi, S.-M., Singh, V.P., 2020. Improving groundwater potential mapping using metaheuristic approaches. Hydrol. Sci. J. 65, 2729–2749.
Regmi, A.D., Devkota, K.C., Yoshida, K., Pradhan, B., Pourghasemi, H.R., Kumamoto, T., Akgun, A., 2014. Application of frequency ratio, statistical index, and weights-of-evidence models and their comparison in landslide susceptibility mapping in Central Nepal Himalaya. Arab. J. Geosci. 7, 725–742.
Robnik-Šikonja, M., Kononenko, I., 1997. An adaptation of Relief for attribute estimation in regression, in: Machine Learning: Proceedings of the Fourteenth International Conference (ICML'97). pp. 296–304.
Saha, A., Pal, S.C., Arabameri, A., Blaschke, T., Panahi, S., Chowdhuri, I., Chakrabortty, R., Costache, R., Arora, A., 2021. Flood susceptibility assessment using novel ensemble of hyperpipes and support vector regression algorithms. Water 13, 241.
Samanta, R.K., Bhunia, G.S., Shit, P.K., Pourghasemi, H.R., 2018a. Flood susceptibility mapping using geospatial frequency ratio technique: a case study of Subarnarekha River Basin. India. Model. Earth Syst. Environ. 4, 395–408.
Samanta, S., Pal, D.K., Palsamanta, B., 2018b. Flood susceptibility analysis through remote sensing, GIS and frequency ratio model. Appl. Water Sci. 8, 1–14.
Samela, C., Albano, R., Sole, A., Manfreda, S., 2018. A GIS tool for cost-effective delineation of flood-prone areas. Comput. Environ. Urban Syst. 70, 43–52.
Shafizadeh-Moghadam, H., Valavi, R., Shahabi, H., Chapi, K., Shirzadi, A., 2018. Novel forecasting approaches using combination of machine learning and statistical models for flood susceptibility mapping. J. Environ. Manage. 217, 1–11.
Shahabi, H., Shirzadi, A., Ghaderi, K., Omidvar, E., Al-Ansari, N., Clague, J.J., Geertsema, M., Khosravi, K., Amini, A., Bahrami, S., 2020. Flood detection and susceptibility mapping using sentinel-1 remote sensing data and a machine learning approach: Hybrid intelligence of bagging ensemble based on k-nearest neighbor classifier. Remote Sens. 12, 266.
Shogrkhodaei, S.Z., Razavi-Termeh, S.V., Fathnia, A., 2021. Spatio-temporal modeling of pm2. 5 risk mapping using three machine learning algorithms. Environ. Pollut. 289, 117859.
Siam, Z.S., Hasan, R.T., Anik, S.S., Noor, F., Adnan, M.S.G., Rahman, R.M., 2021. Study of Hybridized Support Vector Regression Based Flood Susceptibility Mapping for Bangladesh. In: International Conference on Industrial, Engineering and Other Applications of Applied Intelligent Systems. Springer, pp. 59–71.
Souissi, D., Zouhri, L., Hammami, S., Msaddek, M.H., Zghibi, A., Dlala, M., 2020. GIS-based MCDM–AHP modeling for flood susceptibility mapping of arid areas, southeastern Tunisia. Geocarto Int. 35, 991–1017.
Suykens, J.A.K., Vandewalle, J., 1999. Least squares support vector machine classifiers. Neural Process. Lett. 9, 293–300.
Swain, K.C., Singha, C., Nayak, L., 2020. Flood susceptibility mapping through the GIS-AHP technique using the cloud. ISPRS Int. J. Geo-Information 9, 720.
Talha, S., Maanan, M., Atika, H., Rhinane, H., 2019. Prediction of flash flood susceptibility using fuzzy analytical hierarchy process (Fahp) algorithms and Gis: a study case of guelmim region In Southwestern of Morocco. Int. Arch. Photogramm. Remote Sens. Spat. Inf. Sci. 42, 407–414.
Tehrany, M.S., Pradhan, B., Jebur, M.N., 2014. Flood susceptibility mapping using a novel ensemble weights-of-evidence and support vector machine models in GIS. J. Hydrol. 512, 332–343.
Tehrany, M.S., Pradhan, B., Jebur, M.N., 2015a. Flood susceptibility analysis and its verification using a novel ensemble support vector machine and frequency ratio method. Stoch. Environ. Res. risk Assess. 29, 1149–1165.
Tehrany, M.S., Pradhan, B., Mansor, S., Ahmad, N., 2015b. Flood susceptibility assessment using GIS-based support vector machine model with different kernel types. Catena 125, 91–101.
Tehrany, M.S., Jones, S., Shabani, F., 2019a. Identifying the essential flood conditioning factors for flood prone area mapping using machine learning techniques. Catena 175, 174–192.
Tehrany, M.S., Kumar, L., Shabani, F., 2019b. A novel GIS-based ensemble technique for flood susceptibility mapping using evidential belief function and support vector machine: Brisbane. Australia. PeerJ 7, e7653.
Tella, A., Balogun, A.-L., 2020. Ensemble fuzzy MCDM for spatial assessment of flood susceptibility in Ibadan. Nigeria. Nat. Hazards 104, 2277–2306.
Termeh, S.V.R., Kornejady, A., Pourghasemi, H.R., Keesstra, S., 2018. Flood susceptibility mapping using novel ensembles of adaptive neuro fuzzy inference system and metaheuristic algorithms. Sci. Total Environ. 615, 438–451.
Tien Bui, D., Khosravi, K., Li, S., Shahabi, H., Panahi, M., Singh, V.P., Chapi, K., Shirzadi, A., Panahi, S., Chen, W., 2018. New hybrids of anfis with several optimization algorithms for flood susceptibility modeling. Water 10, 1210.
Tiwari, M.K., Chatterjee, C., 2010. Uncertainty assessment and ensemble flood forecasting using bootstrap based artificial neural networks (BANNs). J. Hydrol. 382, 20–33.
Twele, A., Cao, W., Plank, S., Martinis, S., 2016. Sentinel-1-based flood mapping: a fully automated processing chain. Int. J. Remote Sens. 37, 2990–3004. https://doi.org/10.1080/01431161.2016.1192304.
Urbanowicz, R.J., Meeker, M., La Cava, W., Olson, R.S., Moore, J.H., 2018. Relief-based feature selection: Introduction and review. J. Biomed. Inform. 85, 189–203.
Vojtek, M., Vojteková, J., 2019. Flood susceptibility mapping on a national scale in Slovakia using the analytical hierarchy process. Water 11, 364.
Wang, Z., Lai, C., Chen, X., Yang, B., Zhao, S., Bai, X., 2015. Flood hazard risk assessment model based on random forest. J. Hydrol. 527, 1130–1141.
Xu, L., Abbaszadeh, P., Moradkhani, H., Chen, N., Zhang, X., 2020. Continental drought monitoring using satellite soil moisture, data assimilation and an integrated drought index. Remote Sens. Environ. 250, 112028.
Xu, X., Li, J., Tolson, B.A., 2014. Progress in integrating remote sensing data and hydrologic modeling. Prog. Phys. Geogr. 38, 464–498.
Yang, X.-S., 2009. Firefly algorithms for multimodal optimization. International Symposium on Stochastic Algorithms. Springer 169–178.
Young, C.-C., Liu, W.-C., Wu, M.-C., 2017. A physically based and machine learning hybrid approach for accurate rainfall-runoff modeling during extreme typhoon events. Appl. Soft Comput. 53, 205–216.
Zhu, S., Zhou, J., Ye, L., Meng, C., 2016. Streamflow estimation by support vector machine coupled with different methods of time series decomposition in the upper reaches of Yangtze River. China. Environ. Earth Sci. 75, 531.